Dynamics, variability, and change in seasonal precipitation reconstructions for North America

David W. Stahle (corresponding author), Department of Geosciences, University of Arkansas, Fayetteville, AR 72701 dstahle@uark.edu

Edward R. Cook, Lamont-Doherty Earth Observatory, Columbia University, Palisades, NY 10964 drdendro@ldeo.columbia.edu

Dorian J. Burnette, Department of Earth Sciences, University of Memphis, Memphis, TN 38152 djbrntte@memphis.edu

Max C.A. Torbenson, Department of Geosciences, University of Arkansas, Fayetteville, AR 72701 mtorbens@uark.edu

Ian M. Howard, Department of Geosciences, University of Arkansas, Fayetteville, AR 72701 ihowardksu@gmail.com

Daniel Griffin, Department of Geography, University of Minnesota, Minneapolis, MN 55455 griffin9@umn.edu

Jose Villanueva Diaz, Centro Nacional de Investigacion Disciplinaria Relacion Agua-Suelo-Planta-Atmosfera, Lerdo, Mexico villanueva.jose@inifap.gob.mx

Benjamin I. Cook, NASA Goddard Institute for Space Studies, New York, NY 10025 benjamin.i.cook@nasa.gov

Park A. Williams, Lamont-Doherty Earth Observatory, Columbia University, Palisades, NY 10964 williams@ldeo.columbia.edu

Emma Watson, Environment and Climate Change Canada, Toronto M3H 5T4, Canada emma.watson@canada.ca

Early Online Release: This preliminary version has been accepted for publication in *Journal of Climate*, may be fully cited, and has been assigned DOI 10.1175/JCLI-D-19-0270.1. The final typeset copyedited article will replace the EOR at the above DOI when it is published.

David J. Sauchyn, Department of Geography, University of Regina, Regina S4S 0A2, Canada
sauchyn@uregina.ca
Neil Pederson, Harvard Forest, Petersham, MA 10366 mockernut@gmail.com
Connie A. Woodhouse, School of Geography and Development, University of Arizona,
Tucson, AZ 85721 conniew1@email.arizona.edu
Gregory T. Pederson, U.S. Geological Survey, Bozeman, MT 59715 gpederson@usgs.gov
David Meko, Laboratory of Tree-Ring Research, University of Arizona, Tucson, AZ 85721
dmeko@email.arizona.edu
Bethany Coulthard, Department of Geosciences, University of Nevada Las Vegas, Las Vegas,
NV 89154 bethany.coulthard@unlv.edu
Christopher J. Crawford, U.S. Geological Survey, Sioux Falls, SD 57198
cjcrawford@contractor.usgs.gov

December 31, 2019

Revised Manuscript re-submitted to the *Journal of Climate*

Accepted for publication in *Journal of Climate*. DOI 10.1175/JCLI-D-19-0270.1.

Abstract

Cool and warm season precipitation totals have been reconstructed on a gridded basis for North America using 439 tree-ring chronologies correlated with December-April totals and 547 different chronologies correlated with May-July totals. These discrete seasonal chronologies are not significantly correlated with the alternate season and the December-April reconstructions are skillful over most of the southern and western United States and northcentral Mexico, and the May-July estimates have skill over most of the United States, southwest Canada, and northeast Mexico. The strong continent wide El Niño/Southern Oscillation (ENSO) signal embedded in the cool season reconstructions, and the Arctic Oscillation signal registered by the warm season estimates, both faithfully reproduce the sign, intensity, and spatial patterns of these ocean-atmospheric influences on North American precipitation as recorded with instrumental data. The reconstructions are included in the North American Seasonal Precipitation Atlas (NASPA) and provide insight into decadal droughts and pluvials. They indicate that the 16th century megadrought, the most severe and sustained North American drought of the past 500-years, was the combined result of three distinct seasonal droughts each bearing unique spatial patterns potentially associated with seasonal forcing from ENSO, the Arctic Oscillation, and the Atlantic Multidecadal Oscillation. Significant 200- to 500-year long trends toward increased precipitation have been detected in the cool and warm season reconstructions for eastern North America. These seasonal precipitation changes appear to be part of the positive moisture trend measured in other paleoclimate proxies for the East that began due to natural forcing before the industrial revolution and may have recently been enhanced by anthropogenic climate change.

Accepted for publication in *Journal of Climate*. DOI 10.1175/JCLI-D-19-0270.1.

1. Introduction

The consequences of anthropogenic forcing to the global energy balance and regional land cover for climate dynamics, variability, and change over North America are a central focus of climate science and policy (USGCRP 2018). Because instrumental measurements of precipitation and temperature are too short to provide robust characterization of natural climate variability, questions surrounding the anthropogenic forcing of climate have stimulated over 50 years of paleoclimatic research to describe and analyze natural climate variability and change prior to the industrial revolution (e.g., Smerdon et al. 2017). The exactly dated, climate sensitive, and spatially extensive tree-ring chronologies now available for North America have contributed to the reconstruction of pre-instrumental climate (Cook et al. 1999, 2010), particularly the history and dynamics involved in prolonged droughts and pluvials (Woodhouse et al. 2005; Cook et al. 2007; Seager et al. 2007).

The most severe and sustained droughts over North America during the instrumental era were the decadal scale extremes of the 1930s, 1950s, and early 2000s (Fye et al. 2003; Seager 2007). During the 1930s Dust Bowl and the 1950s southern Great Plains Drought, cool season precipitation and temperature anomalies intensified during the warm season when land surface conditions appear to have amplified existing moisture anomalies associated with ocean-atmospheric forcing active in the cool season (Seager and Hoerling 2014). However, the rapid onset or "flash droughts" of 1980 and 2012 (Namias 1982; Mo and Lettenmeier 2015) and other less extreme spring to summer moisture reversals witnessed during the instrumental period document the large uncertainty involved in anticipating warm season moisture levels based on antecedent conditions

Accepted for publication in *Journal of Climate*. DOI 10.1175/JCLI-D-19-0270.1.

during the cool season. This observed variability in seasonal moisture anomalies over North America has motivated the development of long tree-ring chronologies that are well correlated with either cool or warm season moisture, but not with both, in order to extend the limited instrumental observations of seasonal persistence and change deeper into the pre-instrumental era (Stahle et al. 2009; Griffin et al. 2013). These seasonally discrete tree-ring proxies do exist in some numbers, but they have not been employed in systematic gridded reconstructions of both cool and warm season precipitation totals at the continental scale. This article describes the development of cool and warm season precipitation reconstructions for North America and then uses the reconstructions to investigate the climate dynamics, variability, and long-term changes registered in the seasonal estimates over the past several hundred years.

Most North America tree-ring chronologies are sensitive to the long-term soil moisture balance. However, the over 2,500 North American tree-ring chronologies include a subset of chronologies that are correlated with winter to early spring precipitation and another subset sensitive to late spring to mid-summer rainfall, but not both. We have identified these separate tree-ring chronology predictors of cool and warm season precipitation to reconstruct December-April and May-July precipitation totals on a 0.5° latitude/longitude grid over most of North America. The December-April cool season and May-July warm season are the specific months most highly correlated with the moisture response of most available North American tree-ring chronologies that have a distinct seasonal signal. For brevity we refer to these dendroclimatic seasons as the "cool" or "warm" season, but these bioclimatic subdivisions do differ slightly from the standard three-month seasons (DJF, MAM, JJA, SON). The gridded reconstructions are referred to as

Accepted for publication in *Journal of Climate*. DOI 10.1175/JCLI-D-19-0270.1.

115 the North American Seasonal Precipitation Atlas (NASPA). The NASPA seasonal
116 reconstructions calibrate at least 40% of the instrumental precipitation variance over most
117 of North America, extend back over certain regions from 500- to 2,000-years, and provide a
118 new perspective on cool and warm season climate variability and change. These tree-ring
119 estimates of precipitation faithfully record important ocean-atmospheric circulation
120 forcing of cool and warm season precipitation over North America witnessed in the
121 instrumental observations, provide estimates of the seasonal nature of major droughts and
122 pluvials during the pre-instrumental period, and identify statistically significant centennial-
123 scale trend in cool and warm season precipitation over subregions of North America.
124

125 **2. Seasonal moisture signal in North American tree rings**

126 Over 2,500 well dated, climate sensitive tree-ring chronologies are now available for
127 North America, many of which have been contributed to the International Tree-Ring Data
128 Bank (ITRDB) hosted at the paleoclimatology archive of the NOAA National Centers for
129 Environmental Information for open access by the scientific community (Grissino-Mayer
130 and Fritts 1997). A diversity of seasonal climate signals are encoded in these proxy tree-
131 ring chronologies, including positive correlations with warm season rainfall (e.g. Schulman
132 1942; Cleaveland 1986; Therrell et al. 2002; Griffin et al. 2013; Torbenson and Stahle
133 2018), strong positive response to cool season precipitation that recharges the soil
134 moisture column prior to the growing season (e.g., Fritts 1966; Villanueva et al. 2007;
135 Stahle et al. 2009), a negative winter precipitation correlation in the Pacific Northwest due
136 to deep snowpack inhibition of spring-early summer tree growth (Pederson et al. 2011;
137 Welsh et al. 2019), and in certain narrow alpine tree line positions even a positive

Accepted for publication in *Journal of Climate*. DOI 10.1175/JCLI-D-19-0270.1.

correlation with mean monthly temperature during the summer period of high elevation tree growth (e.g., Salzer et al. 2014). Most of these tree-ring chronologies have been previously used to develop the North American Drought Atlas (NADA; Cook et al. 2004), where a point-by-point regression (PPR; Cook et al., 1999) procedure was used to reconstruct the summer (JJA) Palmer Drought Severity Index (PDSI; Palmer 1965) at each of 11,396 grid points with a resolution of 0.5° across the continent (Cook et al. 2010).

The summer PDSI reconstructed for the NADA provides a high-quality estimate of the long-term soil moisture balance conditions that advance or constrain tree growth in most natural forests across North America. The NADA summer PDSI reconstructions have been used to reproduce the detailed temporal and spatial history of continent-wide soil moisture conditions for the past 1,000 years, and for the past 2,000 years over portions of the continent where the oldest moisture-sensitive trees are found. The NADA has been used extensively for analyses of climate variability and change (e.g., Fye et al. 2003; Herweijer et al. 2006; Cook et al. 2010; Cook et al. 2014), investigating the underlying climate dynamics responsible for moisture variability over North America (Cook et al. 2014; Coats et al. 2016; Baek et al. 2017), exploring the role of climate in fire and ecosystem dynamics (Swetnam et al. 2009; Marlon et al. 2017), and the impacts of climate on ancient and modern societies (e.g., Benson et al. 2009; Stahle and Dean 2011; Burns et al. 2014).

Due to the strong month-to-month persistence built into the PDSI formulation to model the slow accumulation and depletion of soil moisture (Palmer 1965; Cook et al. 2007), the PDSI in a given month represents the integration of precipitation inputs and evaporative losses over the course of approximately one year. Because many tree-ring

Accepted for publication in *Journal of Climate*. DOI 10.1175/JCLI-D-19-0270.1.

chronologies from North America integrate climate and soil moisture conditions for several months during and preceding the growing season, the PDSI is an excellent index of the slowly evolving hydroclimate conditions that frequently drive tree growth. However, many North American tree-ring chronologies have a more restricted monthly moisture signal and can be used to estimate seasonal scale changes in climate (Meko and Baisan 2001; Stahle et al. 2009; St. George 2014). For example, time series of blue oak growth in the Mediterranean climate of California have a strong correlation with winter-spring precipitation (e.g., November-April, Meko et al. 2011; September-May; Stahle et al. 2013), while some forest species in the eastern United States are only correlated with late spring and summer moisture levels, especially May-July (e.g., Cook and Jacoby 1977, Elliott et al. 2015, LeBlanc and Stahle 2015). Many conifer and hardwood species also form well-defined spring and summer growth bands (i.e., earlywood and latewood; Figure 1) that can be readily identified and separately measured to produce sub-annual chronologies of earlywood and latewood width that can have discrete seasonal climate signals (e.g., Schulman 1942; Meko and Baisan 2001; Griffin et al. 2013; Torbenson and Stahle 2018; Howard et al. 2019).

To develop the NASPA, all available tree-ring chronologies in Canada (south of 60° N), the United States, Mexico, and western Guatemala were screened for "discrete correlation" with precipitation totals for each season using the Global Precipitation Climatology Centre (GPCC) gridded 0.5° monthly precipitation totals (Becker et al. 2013). Discrete correlation is used here to identify chronologies with a significant precipitation correlation during one season but no significant correlation with the alternate season (p <0.05). Unlike the PDSI, monthly or seasonal precipitation totals do not tend to be strongly

Accepted for publication in *Journal of Climate*. DOI 10.1175/JCLI-D-19-0270.1.

184 correlated and can therefore represent the discrete seasonal hydroclimate conditions that
185 drive tree growth. The two subsets of tree-ring chronologies with discrete seasonal
186 precipitation signals were used to develop separate cool (DJFMA) and warm season (MJJ)
187 precipitation reconstructions for most of North America during the Common Era. Because
188 the correlations between the gridded cool and warm season precipitation reconstructions
189 are still higher in some areas than observed in the instrumental precipitation data, a third
190 set of gridded reconstructions of MJJ precipitation was produced. This was accomplished
191 by using linear regression, grid point by grid point, to remove the antecedent cool season
192 precipitation signal from the warm season reconstructions for the period 1400-2016, thus
193 producing the so-called persistence-free MJJ reconstructions (MJJpf). All three gridded
194 reconstructions are provided (DJFMA, MJJ, and MJJpf), along with the seasonal GPCC
195 precipitation data, and can be investigated online at:
196 http://drought.memphis.edu/NASPA
197 This article presents the DJFMA and the MJJpf reconstructions, but additional analyses of
198 the MJJ precipitation estimates are presented in the Supplemental Material (SM).
199
200 **3. Methods**
201 *a. Instrumental precipitation data*
202 The Global Precipitation Climatology Center-Full Dataset (GPCC_FD)
203 gridded monthly precipitation estimates extending from 1891-2016 were used to calibrate
204 and validate the North American Seasonal Precipitation Atlas
205 (ftp://ftp.dwd.de/pub/data/gpcc/html/fulldata-monthly_v2018_doi_download.html;
206 Becker et al. 2013; Schneider et al. 2018). At each 0.5° grid point on land between 14-55°N

Accepted for publication in *Journal of Climate*. DOI 10.1175/JCLI-D-19-0270.1.

and 50-135°W the precipitation data were totaled for the December-April (DJFMA) cool season and the May-July (MJJ) warm season. Correlation analyses indicate that these seasons optimize the seasonal precipitation signals in the available North American tree-ring data. The seasonal reconstructions were based on power transformed GPCC precipitation data using the method of Hinkley (1977) in order to symmetrize the distribution to quasi normality before using principal components regression (described below). After computing the reconstructions the power transformed precipitation estimates at each grid point were inverse-transformed back to the original units of precipitation (mm). The instrumental and reconstructed precipitation totals were then transformed into the Standardized Precipitation Index (SPI; Guttman 1999) to facilitate the mapping of seasonal precipitation anomalies.

Computing the SPI involved fitting gamma distributions to the cool- and warm-season precipitation data at each grid point. The parameters of the gamma distribution were derived using L-moments, which are analogous to traditional moments but tend to be more robust estimates of summary statistics for probability distributions (Hosking 1990; Guttman et al. 1993). The calculation of these gamma distribution parameters was based on the period 1860-2016, using the reconstructed precipitation data from 1860-1978 and the instrumental data from 1979-2016. The same estimated parameters were then used to compute the gamma probabilities for both the instrumental and reconstructed data at each grid point, but because gamma is undefined for precipitation values equal to zero, a modification to the cumulative probability was warranted:

$$H(x) = q + (1 - q)G(x)$$

Accepted for publication in *Journal of Climate*. DOI 10.1175/JCLI-D-19-0270.1.

where $G(x)$ are the original gamma probabilities, q is the probability of a zero, and $H(x)$ are the final gamma probabilities. Thom (1966) notes that q can be estimated by summing the number of zeroes encountered and dividing by the number of precipitation values, and this method was followed. The final cumulative probabilities at each grid point, $H(x)$, were then transformed into standard normal random variables, Z. These values for Z were the final SPI values (Edwards and McKee 1997).

The monthly precipitation estimates extend back to 1891 at all grid points, but in regions with few station observations the GPCC estimates relax to monthly climatology (Becker et al. 2013), most notably before 1920 (e.g., Figure SM-1). For this reason, the NASPA was calibrated with the seasonal GPCC during the 1928-1978 data rich interval in common with most available tree-ring chronologies. Note that many chronologies end the last quarter of the 20th century when the tree-ring samples were collected. The NASPA reconstructions were then validated from 1901-1927, excluding the last decade of the 19th century when the GPCC estimates are most limited over portions of Canada, the western United States, and Mexico. The few station observations during the early 20th century seen in Figure 2 very likely degrade the statistical validation of the seasonal precipitation reconstructions in some areas, but as discussed below there is strong evidence for the validity of the tree-ring estimates over much of the continent in spite of weak validation statistics in some areas during the 1901-1927 validation period. In fact, the tree-ring reconstructions in the NASPA may provide more accurate estimates of seasonal precipitation during the late-19th and early-20th century in data poor regions such as

Accepted for publication in *Journal of Climate*. DOI 10.1175/JCLI-D-19-0270.1.

252 Sonora (Supplementary Figure SM-1) than is available in the GPCC or any other gridded
253 instrumental precipitation products.

254 Experimental reconstructions of seasonal precipitation were also developed using
255 the Climatic Research Unit monthly precipitation totals (CRU TS4.021; Harris et al. 2014).
256 These CRU-based reconstructions used a similar but not identical subset of North American
257 tree-ring chronologies with discrete seasonal precipitation signals, and the derived
258 reconstructions are similar to those produced using the GPCC data. In fact, because the
259 CRU seasonal precipitation estimates tend to be more spatially smoothed than the GPCC
260 estimates, the calibration and validation results were higher in some regions than those
261 observed when calibrating with the GPCC. Nonetheless, the GPCC was selected for the final
262 reconstructions because of the much larger number of station observations used to
263 compute the gridded monthly estimates (Becker et al. 2013) and the more detailed spatial
264 resolution of the monthly and seasonal precipitation totals.

265

266 *b. Selection of tree-ring chronologies with discrete seasonal moisture signals*

267 The exact monthly to seasonal moisture response of tree-ring chronologies varies
268 across North America due to phenological development associated with the "march of the
269 seasons," spatial differences in the seasonal distribution of precipitation, and many other
270 species and stand level precipitation response factors (e.g., Fritts 1976, Cook et al 1999).
271 But some chronologies are correlated mainly with cool season precipitation (DJFMA), and
272 another separate subset is mainly correlated with warm season precipitation (MJJ).
273 Screening was performed to identify the maximum number of tree-ring chronologies in
274 each seasonal subset, using correlation analysis between the candidate chronologies and

Accepted for publication in *Journal of Climate*. DOI 10.1175/JCLI-D-19-0270.1.

the DJFMA and MJJ precipitation totals (Torbenson 2019). These seasons differ by one month from the traditional climatological definition of winter-spring (DJF-MAM) and summer (JJA) because May moisture can be important to the growth of trees primarily correlated with the cool season, and for other trees mainly correlated with the warm season. Nonetheless, the May moisture response appears to be most commonly associated with warm season sensitive tree-ring chronologies and was therefore included with June and July to represent the warm season in the NASPA reconstructions.

The precise screening procedure used to identify the cool and warm season predictors involved computing the Spearman rank correlation coefficient for all available tree-ring chronologies from North America (i.e., 14-60°N) with DJFMA and MJJ total precipitation at the nine grid points closest to each chronology for the 1928-1978 calibration period. The discretion test was then based on the single grid point out of the nine closest that was most highly correlated for the target season for the over 2,500 tree-ring chronologies. For sites that included total ring width (RW), earlywood width (EW), latewood width (LW), and adjusted LW width chronologies (i.e., LW_a, Meko and Baisan 2001), only the chronology that displayed the strongest correlation with precipitation was chosen for either season. Chronologies that were significantly correlated with DJFMA precipitation ($p < 0.05$), but were not significantly correlated with MJJ precipitation ($p > 0.05$), were then selected as discrete candidate predictors of the cool season moisture. Those significantly correlated only with MJJ were selected as candidate predictors of the warm season precipitation totals. Only EW and LW (or LW_a) chronologies from the same site could be selected for different seasons (e.g., a LW chronology could not be selected for the warm season if the RW chronology was used for the cool season).

Accepted for publication in *Journal of Climate*. DOI 10.1175/JCLI-D-19-0270.1.

298 Using this screening approach, 439 North American tree-ring chronologies were
299 identified with a discrete cool season signal and 547 were identified with a separate warm
300 season response (Figure 3). This objective screening for discrete seasonal predictors was
301 designed to produce two reconstructions, cool and warm season estimates of precipitation
302 across North America useful for investigation of seasonal hydroclimate variability and
303 large-scale climate dynamics. The screening was also intended to produce reconstructions
304 that mimic the magnitude and spatial patterns of persistence between cool and warm
305 season moisture witnessed in instrumental precipitation for North America. This screening
306 minimized the inter-seasonal correlation in the derived reconstructions due to biological
307 growth persistence, which can be inherently strong in subannual chronologies of EW and
308 LW width drawn from the same trees (Torbenson et al. 2016). However, the spatial
309 distribution of selected cool and warm season chronologies clearly differs (Figure 3). The
310 cool season chronologies are strongly concentrated in western North America where
311 winter season soil moisture recharge is most important to growth. In comparison, the
312 warm season chronologies are more uniformly distributed across the continent and reflect
313 those sites and species that are more reliant on the delivery of moisture during the growing
314 season. These spatial limitations of the seasonal proxies have had an important impact on
315 the fidelity of the reconstructions in data sparse regions.
316
317 *c. Tree-ring chronology development*
318 Once the chronologies with discrete seasonal moisture signals were identified using
319 standardized tree-ring series, the raw ring-width data for the selected series were
320 reprocessed to produce ring-width chronologies that preserve common high and medium

Accepted for publication in *Journal of Climate*. DOI 10.1175/JCLI-D-19-0270.1.

frequency variance (i.e., inter-annual to multi-decadal). The raw ring-width data for each measured radius were detrended and standardized using the signal free method (Melvin and Briffa 2008; Cook et al. 2014). The raw ring width data were not available for some sites so the standardized ring width chronologies were used for those sites (i.e., 35 out of 439 for the cool season and 47 out of 547 for the warm season). The sample size varies for each tree-ring chronology, but most chronologies used in the NASPA are based on exactly dated and precisely measured radii from 20 to over 40 trees per site. An age-dependent spline function (Melvin et al. 2007) was fit empirically to each dated and measured radial series, where the stiffness of the spline increases with the age of the tree and in the process tracks the observed trajectory of radial growth more naturally compared to the modified negative exponential curve (Fritts et al. 1969).

To reduce bias in the detrended and standardized ring width indices, the raw ring widths were first power transformed and the indices were calculated by subtraction of the fitted curve value from the measurement value for each year in the time series (Cook and Peters 1997). The biweight robust mean value function (Hoaglin et al. 2000) was then used to compute the mean index tree-ring chronology from the individually detrended and standardized time series from all available trees and radii at each site. Long-term trends in variance of the final signal free chronology were sometimes present due to non-climatic factors such as changes in sample size of dated radii and the loss of ring width variance in some very old trees. Consequently, the variance of the signal free chronologies was detrended (i.e., stabilized) by fitting an age-based spline to the absolute values of the chronology, subtracting the fitted and observed values per year, and restoring the sign of the chronology (Meko et al. 1993). The discrete tree-ring chronologies vary from 160- to

Accepted for publication in *Journal of Climate*. DOI 10.1175/JCLI-D-19-0270.1.

2000-years in length. Based on the number and spatial distribution of predictor tree-ring chronologies (Figure SM-2; Figure 2), the sample size is likely adequate for the seasonal precipitation reconstructions over most of North America from 1400 to 2016.

d. Gridded cool and warm season precipitation reconstructions

Point-by-point regression (PPR; Cook et al. 1999, 2010) was used to develop reconstructions of the cool and warm season precipitation totals at each of 6,812 0.5° grid points over southern Canada, the conterminous United States, and Mexico. PPR involves the fitting of principal components regression (PCR) models based on the tree-ring chronologies located within a given search radius around each grid point of instrumental precipitation data, under the assumption that the chronologies located in the vicinity of each grid point will co-vary with precipitation at that point in a direct and stable manner (Cook et al. 1999). Tree-ring chronologies with a discrete cool or warm season moisture signal in North America were considered for these reconstructions. The instrumental precipitation totals extend from 1891 to 2016, but many tree-ring chronologies were collected much earlier and end in the late 1970s or 1980s. The time interval from 1928 to 1978 was used as the calibration period since it was common to all selected tree-ring chronologies and the instrumental precipitation totals. The instrumental precipitation data available from 1901-1927 were withheld for independent validation of the reconstructions, including Shoemaker F-tests for the equality of variance between the instrumental and reconstructed precipitation totals (Shoemaker 2003; Figure SM-3). The validation interval was not used to screen for discrete seasonal correlation. These calibration and validation

Accepted for publication in *Journal of Climate*. DOI 10.1175/JCLI-D-19-0270.1.

366 periods are similar to those used to produce the NADA (Cook et al. 2004 used 1928-1978
367 and 1900-1927).
368 The reconstructions were computed with a correlation-weighted, ensemble-based
369 version of PPR first developed for the Monsoon Asia Drought Atlas (Cook et al. 2010).
370 There were 16 total ensemble reconstructions for each season, eight ensemble members
371 using predictors from within a 500 km search radius around each instrumental
372 precipitation grid point and eight more ensemble members using predictors from within a
373 1000 km search radius. The 500 km search radius approximates the correlation decay
374 length defined by the *e*-folding level of correlation (*1/e*) between precipitation grid points
375 (New et al. 2000; Mitchell and Jones 2005). The 1000 km search radius allows for the
376 registration of large-scale droughts and pluvials in the seasonal tree-ring proxies, and the
377 relatively sparse and irregular distribution of the tree-ring networks used for seasonal
378 precipitation reconstruction on a regular 0.5° grid (see Figure 3). Because the tree-ring
379 chronologies located by the 1000 km search radius include those in the 500 km search
380 radius, the ensemble average is heavily weighted by the 500 km tree-ring series used. For
381 separate cool and warm season precipitation reconstruction, these large search radii are
382 needed to identify discrete seasonal tree-ring predictors. But they also contribute to the
383 spatial smoothing of the reconstructions.
384 The PPR ensemble method incorporates the covariance between the tree-ring
385 chronologies and the climate target variable by first weighting each tree-ring chronology
386 by some power of its correlation over the calibration period with the climate variable being
387 reconstructed (Cook et al. 2010, 2013b). This is expressed as:
388

Accepted for publication in *Journal of Climate*. DOI 10.1175/JCLI-D-19-0270.1.

$$wTR = uTR * r^p$$

where *uTR* is the unweighted tree-ring chronology in normalized N[0,1] form over the calibration period, *r* is its calibration period absolute correlation with the climate variable being reconstructed, *p* is a power weighting applied to *r*, and *wTR* is the resulting correlation-weighted chronology. This weighting method thus transforms the correlation matrix of tree-ring predictors into a covariance matrix that emphasizes the more heavily weighted (better correlated with climate) tree-ring series. PCR is then conducted using this correlation-weighted covariance matrix. See Cook et al. (2010) for its first use in drought atlas development.

There is no a priori reason why any particular power weighting, *p*, should be optimal. Thus, a range of powers is suggested. Here we use eight powers: {0, 0.1, 0.25, 0.5, 0.67, 1.0, 1.5, 2.0} per search radius. See Cook et al. (2013b) for the functional forms of these correlation weightings. These transformations are monotonic, continuous, and cover the full range of weightings as a function of *r* and chosen *p*. When *p=0, wTR=uTR*. A *p=1.0* indicates a linear weighting by the simple correlation and *p=2.0* indicates a weighting by the square of the correlation. Both have intuitively appealing interpretations regarding relationships between variables, and simple correlation weighting (*p=1.0*) has been used in previous climate reconstructions (e.g., Smerdon et al. 2015; Tierney et al. 2015). PCA applied to each correlation-weighted covariance matrix thus produces a set of orthogonal projection coefficients (PCs) that are weighted differentially by the climate variable being reconstructed. Run this way, PCR produces an ensemble of eight reconstructions per search radius that can be compared and pooled into an ensemble mean reconstruction. This has

Accepted for publication in *Journal of Climate*. DOI 10.1175/JCLI-D-19-0270.1.

been done for the drought atlases produced by Cook et al. (2015), Palmer et al. (2015), and Stahle et al. (2016). Correlation-weighted PCR is used in this way here as well.

Prior to weighting, autoregressive (AR) modeling was applied to the tree-ring chronologies and grid point precipitation data for each season using the "random shock" method of Meko (1981). AR modeling applied this way corrects for differences in persistence between tree rings and precipitation to produce less biased reconstructions of the latter. The AR modeled chronologies found within each search radius were then weighted by their correlations with seasonal precipitation as described above, and principal components analysis (PCA) was used to identify the main modes of covariance between the correlation-weighted chronologies. The time series of PC scores (or amplitudes) were then used as candidate predictors of seasonal precipitation at each grid point (Cook et al. 2015) and the final regression model is based on those predictors with regression t-statistics >1.0. For most of the fitted regression models, this was also equivalent to minimizing the bias-corrected Akaike Information Criterion (AICc, Hurvich and Tsai 1989), but the selected t>1.0 model was sometimes more parsimonious. To extend the reconstructions back in time as the shorter predictor chronologies drop out (e.g., Figure SM-2), PCR was repeated for nested subsets of increasing length (Cook et al. 2004). The variance of each nested subset was scaled to the variance of instrumental precipitation during the calibration period. If a candidate reconstruction nest was correlated below r = 0.2 with the first fully replicated nest (for their full common interval; typically n>150, p<0.01), then that candidate was not used and the grid point reconstruction would end with the previous nest (the skill statistics for these nested subsets are provided at http://drought.memphis.edu/NASPA).

Accepted for publication in *Journal of Climate*. DOI 10.1175/JCLI-D-19-0270.1.

435 The 16 individual ensemble reconstructions for each season (using the eight 500
436 and eight 1000 km members) where averaged with a bi-weight robust mean to provide the
437 initial gridded estimates of cool and warm season precipitation. A 9-point regression
438 kernel based on the Queen's Case adjacency model used in spatial statistics was then
439 applied to each grid point reconstruction to re-estimate and locally smooth the field of
440 reconstructions. In the process, if any of the surrounding eight reconstructions was longer
441 than the center grid point reconstruction, then the center reconstruction was extended or
442 imputed back in time. Based on the Queen's Case adjacency model, and the way in which it
443 locally imputes and provides smoothing to the field, we call this 9-point regression kernel
444 procedure Queen's Case Imputation and Smoothing (QCIS).
445 The QCIS procedure also reduces the number of erratic or inconsistent grid point
446 estimates between adjacent grid points in a given year caused by stochastic variability in
447 the fitted PPR models, and the imputation component more completely fills in spatial
448 discontinuities in the final reconstruction fields. As such, QCIS can also be applied
449 iteratively to previously QCIS-processed fields to increase the spatial smoothing and
450 imputation. For the NASPA, three iterations of QCIS were used to complete the cool and
451 warm season precipitation reconstructions, and the calibration and validation statistics
452 reported here are based on this third iteration.
453 The reconstructions were evaluated on the basis of calibration (1928-1978) and
454 validation period (1901-1927) statistics (Cook et al. 1999), including the calibration period
455 coefficient of multiple determination (CRSQ) and the leave-one-out cross validation
456 reduction of error (CVRE), which is similar to Allen's Prediction Error Sum of Squares
457 (PRESS; Allen 1974). CVRE is a more conservative measure of fractional explained variance

Accepted for publication in *Journal of Climate*. DOI 10.1175/JCLI-D-19-0270.1.

458 and can even go negative, thus making it useful as a regression diagnostics tool (Quan
459 1988). For the verification period, the Pearson correlation coefficient squared (VRSQ), the
460 reduction of error (VRE), and the coefficient of efficiency (VCE) were computed. The CVRE
461 is a less biased measure of the calibrated variance than the CRSQ and may provide the most
462 realistic estimate of the seasonal precipitation skill in the reconstructions only because the
463 instrumental precipitation data are quite limited in some regions of North America during
464 the early 20th century. We note below some additional qualitative 'validation' provided by
465 the similarity between the large-scale teleconnection patterns in instrumental and
466 reconstructed precipitation during the late 19th and 20th century.
467 In spite of the selection of tree-ring predictors with discrete cool or warm season
468 precipitation signal, the correlation between reconstructed DJFMA and MJJ precipitation is
469 still higher at most grid points than the inter-seasonal correlation observed with
470 instrumental cool and warm season totals (Figure SM-4). Persistence-free estimates of
471 reconstructed MJJ precipitation (MJJpf) were therefore calculated at each grid point using
472 the residuals from the regression of reconstructed MJJ precipitation totals on DJFMA totals
473 for the period from 1400-2016 when the seasonal reconstructions are adequately
474 replicated over most of the continent (further described in the Supplementary Material and
475 Figures SM-4 and SM-5). These residuals were then rescaled to units of MJJ precipitation
476 (mm) by regression with the instrumental MJJ precipitation totals at each grid location
477 during the calibration period 1928-1978. The persistence-free MJJ totals were also used to
478 calculate persistence-free records of SPI. The gridded MJJpf estimates of precipitation and
479 SPI are restricted to the period from 1400 to 2016 and are used below with the DJFMA

Accepted for publication in *Journal of Climate*. DOI 10.1175/JCLI-D-19-0270.1.

480 reconstructions for the temporal and spatial analysis of cool and warm season
481 precipitation over the past 600-years.
482
483 **4. Results**
484 *a. Discrete cool and warm season chronologies*
485 A total of 439 tree-ring chronologies with a discrete correlation with December-
486 April precipitation totals were selected for the reconstruction of "cool season" (DJFMA)
487 precipitation (Figure 3a) and 547 chronologies discretely correlated with May-July
488 precipitation were selected for the reconstruction of "warm season" (MJJ) precipitation
489 (Figure 3b). The network of cool season chronologies is extensive over western North
490 America, but is limited over eastern Canada and the northcentral United States (Figure 3a).
491 The warm season chronologies are more evenly distributed across the United States, but
492 are limited over eastern Canada and central Mexico (Figure 3b). Naturally, these gaps in
493 the spatial distribution of seasonal tree-ring chronologies tend to coincide with areas of
494 low reconstruction skill (Figures 4 and 5).
495 Total ring width chronologies dominate the predictor network for both seasons
496 (345 for the cool and 342 for the warm season; Figure 3ab), but the discrete EW and LW
497 chronologies were essential for the cool season precipitation reconstructions in western
498 Canada, the southeastern United States, and Mexico (Figure 3a). For the warm season
499 reconstructions, most of the chronologies used south of 35°N were LW or LWa (Figure 3b).
500 Some of the total RW chronologies are discretely correlated with prior summer
501 precipitation totals (pRW; Figure 3b). These chronologies are located primarily in the
502 northeast and northwestern part of the study area where favorable summer moisture

Accepted for publication in *Journal of Climate*. DOI 10.1175/JCLI-D-19-0270.1.

503 levels can increase stored photosynthate and lead to improved radial growth during the
504 following growing season (Aloni 1991; Watson and Luckman 2002).
505 The strength of the seasonal precipitation signal in the individual cool and warm
506 season tree-ring chronologies is mapped based on the highest Spearman correlation at any
507 point among the nine closest grid points to each chronology for the period 1928-1978
508 (Figure 3 c,d; note that these correlation coefficients do not represent the full
509 reconstruction skill possible with the point-by-point regression methods, as documented in
510 Figures 4 and 5). The Spearman correlations range from 0.26 to 0.90 (and -0.26 to -0.58)
511 for the cool season, with the highest correlations computed for California, Arizona, and the
512 Sierra Madre Occidental of Mexico. The negative correlations in the Pacific Northwest are
513 realistic in terms of bioclimatology and were computed for conifer chronologies inhibited
514 by heavy winter snowpack. The warm season correlations range from 0.26 to 0.73, but
515 correlations above 0.50 are computed widely across the United States and Canada and
516 contribute greatly to warm season reconstruction skill (Figure 3d).
517
518 *b. Calibration and validation of the seasonal precipitation reconstructions*
519 The calibration and validation statistics for the seasonal precipitation
520 reconstructions are mapped for each grid point in Figures 4 and 5. The discrete cool
521 season predictors capture over half of the variance in instrumental December-April
522 precipitation totals for most of western North America extending from southwestern
523 Canada across the western United States and into central Mexico (Figure 4a). Over 40% of
524 the cool season precipitation variance is reconstructed for most of the southcentral and
525 southeastern United States (Figure 4a). The coefficient of multiple determination (CRSQ)

Accepted for publication in *Journal of Climate*. DOI 10.1175/JCLI-D-19-0270.1.

526 computed during the calibration interval 1928-1978 ranges from 0.00 to 0.86 over the
527 entire continent (i.e., all 6,812 grid points). CRSQ is above 0.7 for many grid points in
528 California, but is below 0.2 over much of eastern Canada, Baja California, the Yucatan
529 peninsula, and the Caribbean where few cool season sensitive tree-ring chronologies have
530 been developed (Figure 3a). The weakest calibrated region is in the northern Great Plains
531 and Canada, as shown by the void in the cross-validation reduction of error (CVRE) map
532 associated with negative CVREs (Figure 4b). This is consistent with the low number of
533 chronologies with a significant cool season signal in those regions (Figure 3a,c). However,
534 even the stringent validation statistics computed during the independent interval from
535 1901-1927 indicate strong statistical validation of the cool season precipitation
536 reconstructions over most of subtropical North America extending from California
537 eastward to the southeastern United States where early instrumental observations are
538 abundant, including the square of the Pearson correlation coefficient (VRSQ), the
539 verification period reduction of error (VRE), and the verification period coefficient of
540 efficiency (VCR; Figure 4c-e).

541 The discrete warm season chronologies reproduce over half of the instrumental
542 May-July precipitation variance for most of southern Canada, the United States, and
543 portions of northcentral Mexico (Figure 5a; the CRSQ statistic for the MJJ estimates ranges
544 from 0.00 to 0.74 across all 6,812 grid points). The MJJ precipitation reconstructions are
545 well validated over most of this domain (Figure 5b-e) with the exception of Ontario, the
546 central Rocky Mountains, and northwestern Mexico (Figure 5d,e). A comparison of the
547 CVRE statistics based on the calibration interval 1928-1978 (Figure 5b) with the VRE and
548 VCE computed on the validation period 1901-1927 (Figure 5d,e) indicates that there is

Accepted for publication in *Journal of Climate*. DOI 10.1175/JCLI-D-19-0270.1.

549 useful skill in the tree-ring estimates and that the poor validation period results in these
550 remote regions may again arise in part from limited instrumental precipitation
551 observations during the early 20th century. The spatial distribution of precipitation
552 stations included in the GPCC compilation is illustrated for two decadal episodes over the
553 past 120 years (Figure 2). Very few if any gauge records are available in the areas that
554 exhibit weak validation period statistics for both the cool and warm season precipitation
555 reconstructions during the first decade of the 20th century, including portions of the
556 northern Great Plains (Figure 2a). Even during the 1970s decade of maximum station
557 coverage, many poor performing areas still have the weakest instrumental station coverage
558 (Figure 2b). When the tree-ring calibration and validation statistics are considered in light
559 of the availability of instrumental precipitation observation, the reconstructions may
560 provide useful estimates of seasonal precipitation totals in some data poor areas where the
561 early 20th century validation tests fail (e.g., Sonora, Figures 5 and SM-1). The seasonal
562 reconstructions may also provide useful supplementary data to help constrain early
563 instrumental period reanalyses.
564
565 *c. Dynamical signals in instrumental and reconstructed seasonal precipitation totals*
566 The spatial correlations between the important modes of ocean-atmospheric
567 variability and reconstructed precipitation over North America, and the degree to which
568 the gridded seasonal reconstructions reproduce the teleconnections to cool and warm
569 season precipitation observed in the instrumental data constitutes a stringent test of
570 validity for the NASPA reconstructions. These comparisons are based on the 1928 to 1978
571 calibration interval in common to both the instrumental and reconstructed precipitation

Accepted for publication in *Journal of Climate*. DOI 10.1175/JCLI-D-19-0270.1.

572 data. Because instrumental measurements of ENSO and other modes of circulation in some
573 cases begin in the mid-19th century, we also correlate these earliest circulation indices with
574 the reconstructed seasonal precipitation totals during the 19th and early 20th century
575 largely prior to the availability of gridded instrumental precipitation data for North
576 America. These "pre-calibration" correlations are all based on the 1872-1927 period and
577 provide further insight into the fidelity of the reconstructions and the stability of large-
578 scale climate teleconnections to North America at the beginning of instrumental
579 observations and prior to the heaviest anthropogenic forcing of regional to global climate.
580 The modes of ocean-atmospheric circulation tend to be most energetic and teleconnections
581 most intense during the cool season, but we describe important circulation influences on
582 both cool and warm precipitation using the instrumental and reconstructed totals.
583
584 *i. Cool season*
585 The strongest circulation influence on cool or warm season precipitation over North
586 America is associated with ENSO. There are highly significant point-wise positive
587 correlations (p<0.001) between the November-February (NDJF) extended Multivariate
588 ENSO index (eMEI; Wolter and Timlin 2011) and cool season precipitation totals over
589 subtropical North America in both the instrumental and reconstructed data, particularly
590 over northern Mexico and the southwestern United States (Figure 6ab). There is a
591 significant negative correlation between the NDJF eMEI and cool season precipitation over
592 the Pacific Northwest, southern Canada, and Ohio Valley (Figure 6ab). Instrumental and
593 reconstructed cool season precipitation totals are also correlated with indices of the
594 Pacific/North American pattern (PNA; Figure SM-6) and the Pacific Decadal Oscillation

Accepted for publication in *Journal of Climate*. DOI 10.1175/JCLI-D-19-0270.1.

(PDO; Figure SM-7), but the spatial patterns of correlation tend to be weaker and closely resemble the ENSO teleconnection. However, the PDO in particular may interact with other modes of ocean-atmospheric forcing to result in significant impact on cool season precipitation over North America (e.g., Gershunov and Barnett 1998).

The reconstructions reproduce the spatial pattern of the ENSO teleconnection to instrumental precipitation with great fidelity, including the detailed geographical structure to the signal over the Pacific Northwest and southern Mexico. However, the area and magnitude of correlation over northern Mexico and the Southwest is stronger, and the correlation over Florida is weaker in the reconstructions than in the instrumental data (Figure 6a-c). These differences are due in part to the nature of the PPR reconstruction method and the search radii that were used. The enhanced ENSO signal over the "TexMex" sector may also be due in part to the additional though weak October-November precipitation response in of some the predictor tree-ring chronologies from the region (not shown), correlation with seasonal temperature conditions in some tree-ring data, and the limited instrumental observations from Mexico before 1950 (e.g., Stahle et al. 2016).

The pattern and intensity of the ENSO signal in cool season precipitation during the late 19th and early 20th century (Figure 6c) is very similar to the 20th century response (Figure 6a,b), although the significant positive correlations weakened over California while they strengthened across the eastern United States. The negative ENSO correlation observed in the Ohio Valley during the period 1928-1978 was not present in the reconstructions from 1872-1927 (Figure 6c), as noted by Cole and Cook (1998) and Torbenson et al. (2019). These comparisons suggest that the ENSO signal to North America

Accepted for publication in *Journal of Climate*. DOI 10.1175/JCLI-D-19-0270.1.

617 has been most stationary only over the TexMex and Pacific Northwest sectors during the
618 past 146-years.

619 The North Atlantic Oscillation (NAO) is the sea level pressure gradient between the
620 subpolar low and subtropical high over the North Atlantic that influences cool season
621 weather and climate in eastern North America and especially Europe (Hurrell et al. 2003).
622 The NAO for DJFMA is significantly correlated with instrumental and reconstructed cool
623 season precipitation over the Ohio and Lower Mississippi Valleys, where DJFMA
624 precipitation tends to be enhanced during the positive phase of the NAO (Figure SM-8a,b;
625 https://crudata.uea.ac.uk/cru/data/nao/nao.dat). This enhanced cool season precipitation
626 response to the positive NAO is consistent with analyses of instrumental data and some
627 model simulations (Durkee et al. 2008; Ning and Bradley 2016; Whan and Zwiers 2017). It
628 is also consistent with analyses of instrumental and tree-ring reconstructed Palmer
629 drought indices (Fye et al. 2006). However, the NAO correlation with reconstructed DJFMA
630 precipitation weakened over the central United States during the late 19th and early 20th
631 century (Figure SM-8c). The reason for this non-stationarity is not clear, but the NAO
632 teleconnection to instrumental and reconstructed DJFMA precipitation also weakened
633 during the earliest period of instrumental GPCC precipitation observations from 1892 to
634 1927 (not shown).

635 The Arctic Oscillation (AO) is an annular mode of zonal circulation between 35 and
636 55 N (Ambaum et al. 2001). The NAO and PNA are related to the AO (Ambaum et al. 2001),
637 and the correlation between indices of the NAO and AO for the winter to mid-spring season
638 (DJFMA) is r =0.68 (p <0.001; 1928-1978). Consequently, the AO is also positively
639 correlated with instrumental and reconstructed cool season precipitation totals over the

Accepted for publication in *Journal of Climate*. DOI 10.1175/JCLI-D-19-0270.1.

640 Ohio Valley during the calibration period 1928-1978 similar to the pattern of correlation
641 with the NAO (not shown). However, the correlation between the AO and warm season
642 precipitation reverses sign from the cool to warm season when the May-June AO index
643 becomes negatively correlated with MJJ and MJJpf precipitation over the central United
644 States. This change in the response of precipitation to the AO may be broadly due to the
645 poleward migration of the jet stream from the cool to warm season.
646
647 *ii. Warm season*
648 The AO index is computed as the leading PC of monthly mean Northern Hemisphere
649 sea level pressure field (20-90°N; Thompson and Wallace 2000). The AO tends to weaken
650 in the warm season, but a significant negative correlation between the summer AO index
651 and summer precipitation over the central United States has nevertheless been previously
652 detected (Hu and Feng 2009). This negative AO signal is also detected in the instrumental
653 and reconstructed MJJ or MJJpf precipitation totals and SPI extending from the Great Plains
654 across the Ohio Valley and into the northeastern United States (Figures 7a-c, SM-9a,b). The
655 strongest correlations with MJJ totals are computed with just the May-June AO index
656 (Figures 7, SM-9), but the full warm season (MJJ) AO index is also well correlated with
657 gridded MJJ precipitation in the instrumental and reconstructed data (not shown).
658 The correlation between the May-June AO index during the 1872-1927 period is
659 similar to the correlations for 1928-1978 (Figure 7a-c), indicating that the Arctic
660 Oscillation has been an important factor in warm season precipitation variability over
661 North America for the past 150-years. The positive phase of the AO is associated with a
662 northward shift of the jet stream and with subsidence, moisture divergence, and reduced

Accepted for publication in *Journal of Climate*. DOI 10.1175/JCLI-D-19-0270.1.

663 warm season rainfall over the central United States (Hu and Feng 2009) where the
664 instrumental and reconstructed data are negatively correlated with the AO. The AO is also
665 positively correlated with MJJ precipitation totals over southwestern North America
666 (Figure 7) and may therefore play a role in promoting the North American Monsoon. The
667 NAO index averaged for May-June is also significantly and negatively correlated with
668 instrumental and reconstructed MJJ precipitation over the central United States from 1892-
669 1927 (similar to the AO; not shown). This negative NAO correlation weakens from 1928-
670 1978, but still contrasts with the positive DJFMA NAO teleconnection to cool season
671 precipitation over this region (Figure SM-8).
672 The influence of the Atlantic Multidecadal Oscillation (AMO), detrended area
673 average SSTs in the Atlantic north of 0° (Enfield et al. 2001), has also been detected in
674 warm season precipitation totals, primarily over northern Mexico and the Southwest
675 (McCabe et al. 2004; Seager et al. 2007). The annual average AMO (Aug-Jul:
676 http://www.esrl.noaa.gov/psd/data/timeseries/AMO/) is negatively correlated with
677 instrumental and reconstructed MJJ and MJJpf precipitation over portions of northern
678 Mexico and the southern United States for the calibration period (Figure SM-10a-c), but
679 only over the Southwest during the pre-calibration interval (Figure SM-10d,e). The AMO is
680 not strongly correlated with cool season precipitation over North America (not shown).
681 Due to the strong persistence in the AMO index, composite analyses of the precipitation
682 reconstructions were also computed for the phases of the AMO. Modestly dry conditions
683 prevailed over southwestern North America during the positive phases of the AMO (i.e.,
684 1857-1901, 1931-1963) and slightly wet conditions during negative phases (1902-1930,
685 1964-1995; not shown), consistent with the correlation analyses in Figure SM-10.

Accepted for publication in *Journal of Climate*. DOI 10.1175/JCLI-D-19-0270.1.

686

687 *d. Cool and warm season precipitation variability over North America*

688 For a time series perspective on the seasonal precipitation reconstructions, the cool
689 and warm season precipitation estimates are plotted from 1400-2016 for nine 10 x 10°
690 regions of North America in Figures SM-11 and SM-12, including the southcentral United
691 States (Figures 8, SM11c, and SM-12c) where the cool and warm season reconstructions
692 are well calibrated and validated [Figures 4 and 5; and where the persistence-free warm
693 season estimates are also correlated with instrumental MJJ precipitation (Figure SM-5a,b)].
694 The reconstructions for the southcentral United States indicate more frequent and severe
695 cool and warm season drought during the 15th century (Figure 8a-b), although reduced
696 sample size and scaling of the nested reconstructions may impact the intensity of these
697 ancient droughts and deserve further study. The regional reconstructions indicate large
698 seasonal differences in the severity and persistence of certain moisture regimes, including
699 the pluvial in the early-19th century that was one of the wettest warm season decades of
700 the past 600 years, but was near normal during the cool season (1803-1812; Figure 8a-b).
701 The warm season reconstructions also exhibit significant linear trends in MJJpf
702 precipitation totals from 1400-2016 (p = 0.01; Figure 8b). Long-term trends are less
703 pronounced in the cool season reconstruction for the southcentral United States, but the
704 20th century is here estimated to have been the wettest 100-year cool season episode since
705 1400 (Figure 8a).

706 The mid-19th century drought was one of the most severe pre-industrial droughts of
707 the past 500 years based on the long-term soil moisture balance reconstructions in the
708 NADA (Fye et al. 2003; Herweijer et al. 2004). The NASPA seasonal precipitation

Accepted for publication in *Journal of Climate*. DOI 10.1175/JCLI-D-19-0270.1.

709 reconstructions indicate that dry conditions were widespread over North America during
710 both the cool and warm seasons from 1855 to 1864 (Figure 9). However, the center of
711 intense drought during the mid-19th century appears to have shifted from the Southern
712 Plains in the cool season into the Northern Plains-Northern Rockies during the warm
713 season (Figure 9a,b). Near normal to above average MJJpf precipitation is estimated for the
714 lower Mississippi and Ohio Valleys in strong contrast to the intense decadal drought
715 reconstructed for the cool season during the mid-19th century (Figure 9a,b).
716 Out-of-phase seasonal moisture conditions lasting 10-years or longer are not
717 common in the reconstructions or in the instrumental record, but dryness prevailed in the
718 warm season over the eastern United States during the mid-18th century when cool season
719 precipitation was near normal (Figure 9c,d). The intense pluvial over western North
720 America during the final decade of the pre-Columbian era (1483-1492) extended from
721 Mexico to the northern Great Plains during the cool season, but dry conditions developed
722 during the warm season over much of this same sector of western North America in one of
723 the largest decade-scale reversals of cool to warm season precipitation in the new
724 reconstructions (Figure 9e,f).
725 The 16th century megadrought was the most severe and sustained drought of the
726 past 500-years based on the gridded PDSI reconstructions in the NADA (Stahle et al. 2000;
727 Cook et al. 2004). The 16th century megadrought impacted most of North America during
728 the mid- to late-1500s (Meko et al. 1995; Stahle et al. 2007) and has been associated with
729 intense and prolonged cool conditions in the equatorial Pacific (Cook et al. 2018). The new
730 NASPA reconstructions indicate that the 16th century megadrought may actually have been
731 two or even three separate droughts, possibly involving different climate dynamics. The

Accepted for publication in *Journal of Climate*. DOI 10.1175/JCLI-D-19-0270.1.

start and end dates of the megadrought varied spatially during the late 16th century (Stahle et al. 2007; Cook et al. 2018), but from 1568 to 1591 cool season drought prevailed over the Southwest, northern Mexico, and the eastern United States along with wetness over southern Mexico (Figure 10a). Warm season drought prevailed over the midwestern United States and persisted from winter to summer over Arizona and Sonora (Figure 10b). The seasonal and spatial patterns of these late 16th century precipitation regimes bear some resemblance to the continent-wide teleconnection anomalies associated with La Niña events during the cool season (note Figures 6a,b and 10a), the Arctic Oscillation during the warm season over the central United States (Figures 7a-c and 10b), and possibly the Atlantic Multidecadal Oscillation for the warm season over the Southwest (Figures 10b,c and SM-10).

By design, the long-term soil moisture reconstructions developed for the North American Drought Atlas (Cook et al. 1999; 2010) integrate the three regional and seasonal droughts of the late 16th century into a prolonged episode of coast-to-coast dryness (Figure 10c; Cook et al. 2018). But this integration may obscure part of the explanation for this multidecadal episode of severe and sustained drought. The NASPA reconstructions in Figure 10 suggest that the continent-wide megadrought of the late 16th century may have developed from the convergence of cool season drought over subtropical North America involving ENSO with warm season droughts over the central and southwestern United States involving the AO and AMO. What is not clear, however, is how these three modes of atmospheric circulation, which are known to influence North American regional precipitation totals on interannual time scales, may have each persisted or recurred with

Accepted for publication in *Journal of Climate*. DOI 10.1175/JCLI-D-19-0270.1.

754 sufficient frequency to have influenced the 24-year moisture regimes reconstructed for the
755 late-16th century.
756
757 *e. Secular trend in seasonal precipitation over North America*
758 The positive trend in reconstructed warm season precipitation totals over the
759 southcentral United States (Figure 8b) is part of a significant wetness trend reconstructed
760 for the cool and warm seasons over much of eastern North America. However, this large-
761 scale wetness trend appears to have been longer and stronger in the warm season. The
762 precipitation reconstructions at each grid point were tested for linear trend using two time
763 intervals that appear to include some of the strongest and most widespread changes in
764 reconstructed precipitation for each season. The robust Theil-Sen slope statistic is mapped
765 for each gridded cool season reconstruction for the interval 1800-2016 (Figure 11a) and
766 for the persistence-free warm season reconstructions from 1500-2016 (Figure 11b).
767 Significant long term and positive trend is identified over eastern North America during the
768 cool and especially the warm seasons. Groisman et al. (2004) also note stronger warm
769 season precipitation trend in instrumental observations for the eastern United States from
770 1900 to 2002. Hoerling et al. (2016) identify positive trend in heavy warm season
771 precipitation events over the Midwest and Northeast (1979-2013). And NOAA's National
772 Centers for Environmental Information indicate significant positive trend (p<0.05) for
773 summer precipitation over the Midwest, but no significant trend over the 48 United States
774 in winter from 1895-2018 (www.ncdc.noaa.gov/temp-and-precip/us-trends/).
775 A long-term trend in wetness over eastern North America has been previously
776 identified by paleoclimate and modern climate research, including trend at millennial

Accepted for publication in *Journal of Climate*. DOI 10.1175/JCLI-D-19-0270.1.

(Shuman and Marsicek 2016), centennial (Pederson et al. 2013; Newby et al. 2014), and decadal time scales (Groisman et al. 2004, 2005; Seager et al. 2012; Bishop et al. 2019). The millennial scale trends have been related to large-scale cooling and increased effective moisture over the Northern Hemisphere since the mid-Holocene (Shuman and Marsicek 2016), but the more recent wetness trends are not well understood (Pederson et al. 2013). Anthropogenic warming and wetting of the atmosphere may have contributed to the positive trend in total precipitation over the eastern United States in recent decades, and to the increase in very heavy precipitation events in the midlatitudes (Groisman et al. 2005). However, other analyses suggest that the trend in precipitation, extreme precipitation, or water vapor in the East may have arisen only from internal atmospheric variability (e.g., Seager et al. 2012; Kunkle et al 2013; Hoerling et al. 2016). Because the trends in reconstructed seasonal totals begin before the onset of the industrial revolution and heavy anthropogenic climate forcing, natural variability may be implicated in at least the initiation of these long-term precipitation changes in eastern North America.

These tests of trend in the precipitation reconstructions are sensitive to the time interval of analysis, and the area of significant negative trend in reconstructed cool season precipitation over the Pacific Northwest is more widespread when based on the 300-year period from 1700-2016 (not shown; see also Pederson et al. 2011). The reconstructed precipitation trends are also modest in terms of the absolute change in total precipitation. The warm season trend in MJJpf precipitation from 1500 to 2016 for the southcentral United States (Figure 8b) is 0.063mm/yr ($p < 0.01$), or approximately 10.8% of the long-term warm season mean from 1400 to 2016. The shorter trend in cool season precipitation

Accepted for publication in *Journal of Climate*. DOI 10.1175/JCLI-D-19-0270.1.

for the southcentral United States from 1800 to 2016 (Figure 8a) was 0.267mm/yr ($p < 0.05$), or some 15.0% of the reconstructed cool season mean from 1400 to 2016.

The reconstructions of seasonal precipitation are inevitably based on many fewer tree-ring chronologies during the earliest years of record in the nested estimates. This means that there is a greater likelihood of extrapolating regional tree-ring estimated precipitation information over a larger spatial domain for the earliest years in the NASPA. But the reconstructions nonetheless provide important and spatially specific insight into centennial scale variability in seasonal precipitation totals. The need to better understand these long-term precipitation changes, both from the perspective of climate dynamics and water resources planning, justifies a concerted effort to expand the collection of millennium-long tree-ring chronologies sensitive to cool or warm season moisture, particularly over eastern North America.

5. Discussion and Conclusions

The new tree-ring reconstructions of cool, warm, and persistence-free warm season precipitation are based on a subset of North American tree-ring chronologies with discrete seasonal moisture signals. The reconstructions calibrate at least 40% of the variance for both December-April (cool season) and May-July (warm season) precipitation totals over a large portion of North America for up to 2,000-years. The areas of lowest calibration and validation skill in both the cool and warm season reconstructions are located where few seasonal tree-ring chronologies or few instrumental observations are available. Development of additional long tree-ring chronologies with discrete seasonal precipitation

Accepted for publication in *Journal of Climate*. DOI 10.1175/JCLI-D-19-0270.1.

821 signals is feasible and would lead to improved cool and warm season moisture
822 reconstructions for North America.
823 The new reconstructions represent the first spatially explicit estimates of both cool
824 and warm season precipitation amounts over much of the North American continent and
825 are most strongly replicated with seasonally discrete tree-ring chronologies during the past
826 600 years. The reconstructions for the cool and warm seasons extend as far back as 2,000
827 years where discrete seasonal predictors are available, but the persistence-free warm
828 season reconstructions are confined to the period 1400-2016. The reconstructions
829 estimate strong, widespread, and seasonally persistent drought and wetness regimes, as
830 well as other episodes of cool to warm season precipitation reversals that may signify
831 unusual configurations of ocean-atmospheric circulation. In both seasons, tree-ring
832 reconstructed precipitation over most of North America recorded more severe and
833 sustained decadal droughts than were witnessed during the modern instrumental era,
834 helping to document the range of persistent and widespread dryness that was possible
835 under natural conditions prior to heavy anthropogenic forcing of regional and global
836 climate.
837 The seasonal precipitation reconstructions are significantly correlated with indices
838 of ENSO, the PDO, PNA, NAO, and the AO in winter, and with the AO and AMO during
839 summer. The spatial correlations faithfully reproduce the teleconnection patterns present
840 in the instrumental precipitation data and provide strong dynamical justification for the
841 extraction of discrete seasonal climate information from the network of North American
842 tree-ring chronologies. In fact, the sign of significant seasonal precipitation correlations
843 with the AO reverses from the cool to warm season over the central United States as the jet

Accepted for publication in *Journal of Climate*. DOI 10.1175/JCLI-D-19-0270.1.

stream and mean storm track shift poleward with the onset of summer. This change in the sign of AO forcing of seasonal precipitation is also detected in the long-term soil moisture balance reconstructions available in the NADA, but the magnitude and area of significant correlations with seasonal AO indices (i.e., DJFMA and MJ) are much lower in the instrumental and reconstructed JJA PDSI in the NADA.

The cool season reconstructions indicate that the ENSO influence on December-April precipitation was as strong during the late 19th and early-20th century as it was during the mid-20th century, especially over northern Mexico where the teleconnection is arguably the strongest and most stable over time (Stahle et al. 2016; Torbenson et al. 2019). The Arctic Oscillation has the strongest correlation with instrumental and reconstructed warm season precipitation in both the calibration period (1928-1978) and with the reconstructed MJJ and MJJpf totals during the late-19th and early-20th century. Warm season precipitation is suppressed over most of the continent during the positive phase of the AO, but it is enhanced over northern Mexico and the Southwest, especially in the reconstructed warm season totals. The consistency of the ocean-atmospheric teleconnections to seasonal precipitation in both the instrumental and reconstructed totals provides important validation of the tree-ring reconstructions from the perspective of the internal climate dynamics that drive moisture variability across North America. These teleconnection results, coupled with the calibration and validation statistics, also indicate that the tree-ring reconstructions of seasonal precipitation may constitute the best seasonal precipitation estimates currently available for certain remote areas of Canada, the western United States, and Mexico during the early 20th century when station observations were limited or non-existent.

Accepted for publication in *Journal of Climate*. DOI 10.1175/JCLI-D-19-0270.1.

867 The seasonal reconstructions indicate significant positive trend in cool and warm
868 season precipitation that impacted most of eastern United States. Enhanced precipitation
869 amounts have been documented for eastern North America on an annual basis with other
870 paleoclimate proxies (Pederson et al. 2013). The wetness trend in tree-ring reconstructed
871 warm season precipitation began at least 500-years ago, and some 200-years ago for cool
872 season precipitation, and both may have been enhanced in recent decades by
873 anthropogenic activity. The dynamics responsible for these moisture trends may involve a
874 combination of factors related to anthropogenic warming (Groisman et al. 2005), but the
875 reconstructions indicate that cool and warm season precipitation trend began well before
876 the industrial revolution and may also involve internal climate variability. The seasonal and
877 spatial differences in reconstructed precipitation trend might provide insight into the
878 underlying factors responsible for increasing precipitation over eastern North America.
879 The 16th century megadrought was the most severe, sustained, and continent-wide
880 drought of the past 500-years based on the tree-ring reconstructions of PDSI provided by
881 the North American Drought Atlas (Cook et al 2010), but the North American Seasonal
882 Precipitation Atlas indicates that it may have been the combined result of three spatially
883 distinct seasonal droughts. The seasonal moisture anomalies associated with these three
884 co-occurring late-16th century droughts resemble the teleconnection patterns associated
885 with ENSO, the AO, and the AMO in the instrumental and reconstructed precipitation data
886 during the 19th and 20th centuries. If these modes of ocean-atmospheric forcing of North
887 American precipitation were active in the late-16th century, then they may have
888 contributed to the megadrought. Many examples of seasonal differences in the spatial
889 pattern of precipitation can be found in the NASPA at inter-annual, decadal, and

Accepted for publication in *Journal of Climate*. DOI 10.1175/JCLI-D-19-0270.1.

890 multidecadal time scales, and provide a rich source of precipitation variability that should
891 be useful for investigations of North American climate dynamics and change during the late
892 Holocene.
893

Accepted for publication in *Journal of Climate*. DOI 10.1175/JCLI-D-19-0270.1.

894 **Interactive web-based analysis of the North American Seasonal Precipitation Atlas**

895 The instrumental and tree-ring reconstructed cool and warm season precipitation
896 data can be accessed at: http://drought.memphis.edu/NASPA/
897 where it is possible to create maps of instrumental or reconstructed DJFMA, MJJ, MJJpf
898 precipitation totals or standardized precipitation indices, plot time series for single points
899 or user selected regional averages, create correlation maps, access the calibration and
900 validation statistics for all nested reconstructions, and many other analyses.

901

902

903 **Data availability**

904 The tree-ring data, both raw ring width measurement series and the derived
905 chronologies, the instrumental cool and warm season gridded GPCC precipitation data, and
906 the gridded seasonal precipitation reconstructions are all available at:
907 ITRDB at NOAA Paleo (https://www.ncdc.noaa.gov/data-access/paleoclimatology-
908 data/datasets/tree-ring).

909

910

911 **Acknowledgements**

912 NSF grant numbers GEO/ATM-0753399, AGS-1266014, AGS-1266015, AGS-1301587, AGS-
913 1502224, and AGS-1702894. We thank Rodolfo Acuna Soto, Chris Baisan, Jordan Burns,
914 Julian Cerano Paredes, Malcolm Cleaveland, Jeff Dean, Falko Fye, Paul Krusic, Mark
915 Losleban, Martin Munro, Richard Seager, Jason Smerdon, Scott St. George, Paul Szejner,
916 Matt Therrell, Gene Wahl, for assistance and advice, and the many contributors to the

Accepted for publication in *Journal of Climate*. DOI 10.1175/JCLI-D-19-0270.1.

International Tree-Ring Data Bank, particularly John King, Peter Brown, Jesse Edmondson, Lisa Graumlich, Richard Guyette, D. Rubino, Bill Callahan, Brian Luckman, Brendan Buckley, Mike Stambaugh, Tom Swetnam, Troy Knight, and Tony Caprio. The editor and three peer reviews provided helpful suggestions that have improved this article. Any use of trade, firm, or product names is for descriptive purposes only and does not imply endorsement by the U.S. Government.

Lamont-Doherty Earth Observatory contribution number xxxx.

Accepted for publication in *Journal of Climate*. DOI 10.1175/JCLI-D-19-0270.1.

927 **References Cited**

928 Allen, D.M., 1974: The relationship between variable selection and data augmentation and a
929 method for prediction. *Technometrics*, **16**, 125–127.

930 Aloni, R., 1991: Wood formation in deciduous hardwood trees. In *Physiology of Trees*, edited
931 by A. S. Raghavendera, pp. 175–197. John Wiley & Sons, New York, NY.

932 Ambaum, M.H.P., B.J. Hoskins, and D.B. Stephenson, 2001: Arctic Oscillation or North
933 Atlantic Oscillation? *J. Climate*, **14**, 3495-3507.

934 Baek, S.H., J.E. Smerdon, S. Coats, A.P. Williams, B.I. Cook, E.R. Cook, R. Seager, 2017:
935 Precipitation, temperature, and teleconnection signals across the combined North
936 American, Monsoon Asia, and Old World Drought Atlases. *J. Climate,* **30**, 7141-7155.

937 Becker, A., P. Finger, A. Meyer-Christoffer, B. Rudolf, K. Schamm, U. Schneider, and M. Ziese,
938 2013: A description of the global land-surface precipitation data products of the Global
939 Precipitation Climatology Centre with sample applications including centennial (trend)
940 analysis from 1901–present. *Earth Syst. Sci. Data,* **5**, 71-99.

941 Benson, L.V., T.R. Pauketat, and E.R. Cook, E.R. 2009. Cahokia's boom and bust in the
942 context of climate change. *American Antiquity,* **74**, 467-483.

943 Bishop, D., A.P. Williams, R. Seager, A.M. Fiore, B.I. Cook, J.S. Mankin, D. Singh, J.E. Smerdon
944 and M.P. Rao, 2018: Investigating the causes of increased Twentieth-Century precipitation
945 over the southeastern United States, *J. Climate*, 32, 575-590.

946 Burns, J.N., R. Acuna-Soto, and D.W. Stahle, 2014: Drought and epidemic typhus, central
947 Mexico, 1655-1918. *Emerging Infectious Diseases,* **20**, 442-447.

948 Cleaveland, M.K., 1986: Climatic response of densitometric properties in
949 semiarid site tree rings. *Tree-Ring Bull.,* **46**, 13–29.

Accepted for publication in *Journal of Climate*. DOI 10.1175/JCLI-D-19-0270.1.

950 Coats, S., J.E. Smerdon, B.I. Cook, R. Seager, E.R. Cook, K.J. Anchukaitis, 2016: Internal
951 ocean-atmosphere variability drives megadroughts in western North America. *Geophys.*
952 *Res. Lett.,* **43**, 9886-9894.
953 Coats, S., B.I. Cook, J.E. Smerdon, and R. Seager, 2015: Winter-to-summer precipitation
954 phasing in southwestern North America: A multi-century perspective from paleoclimatic
955 model-data comparisons, *J. Geophys. Res*., **120**, 8052-8064, doi:10.1002/2015JD023085.
956 Cook, B., J. Smerdon, R. Seager and S. Coats, 2014: Global warming and 21st century drying.
957 *Climate Dynamics*, **43**, 2607-2627, doi:10.1007/s00382-014-2075-y.
958 Cook, B.I., A.P. Williams, J.E. Smerdon, J.G. Palmer, E.R. Cook, D.W. Stahle, and S. Coats, 2018:
959 Cold Tropical Pacific Sea Surface Temperatures During the Late
960 Sixteenth-Century North American Megadrought. *J. Geophys. Res: Atmospheres*, **123**,
961 11,307–11,320. https://doi.org/10.1029/2018JD029323
962 Cook, E.R., and G.C. Jacoby, 1977: Tree-ring-drought relationships in the Hudson Valley,
963 New York. *Science*, **198**, 399-401.
964 Cook, E.R. and K. Peters, 1997: Calculating unbiased tree-ring indices for the study of
965 climatic and environmental change. *The Holocene*, 7, 359-368.
966 Cook, E.R., C. Woodhouse, C.M. Eakin, D.M. Meko, and D.W. Stahle, 2004: Long-term aridity
967 changes in the western United States. *Science,* **306**, 1015-1018.
968 Cook, E.R., R. Seager, M.A. Cane, and D.W. Stahle, 2007: North American Drought:
969 reconstructions, causes, and consequences. *Earth Science Review,* **81**, 93-134.
970 Cook, E. R., R. Seager, R. R. Heim Jr, R. S. Vose, C. Herweijer, and C.Woodhouse, 2010:
971 Megadroughts in North America: placing IPCC projections of hydroclimatic change in a
972 long-term palaeoclimate context*. J. Quaternary Science,* **25**, 48–61.

Accepted for publication in *Journal of Climate*. DOI 10.1175/JCLI-D-19-0270.1.

973 Cook, E.R., K.J. Anchukaitis, B.M. Buckley, R. D'Arrigo, G.C. Jacoby, W.E. Wright, 2010: Asian
974 monsoon failure and megadrought during the last millennium. *Science,* **328**, 486-489
975 Cook, E.R., Palmer, J.G., Ahmed, M., Woodhouse, C.A., Fenwick, P., Zafar, M.U., Wahab, M.
976 Khan, N. 2013a: Five centuries of upper Indus River flow from tree rings. *J. Hydrology*, **486**,
977 365–375.
978 Cook, E.R., Krusic, P.J., Anchukaitis, K.J., Buckley, B.M., Nakatsuka, T., Sano, M., and Asia2k
979 members, 2013b: Tree-ring reconstructed summer temperature anomalies for temperate
980 East Asia since 800 C.E. *Climate Dynamics*, **41**, 2957-2972. https://doi: 10.1007/s00382-
981 012-1611-x.
982 Cook, E. R., P. J. Krusic, and T. Melvin, 2014: Program RCSigFree. Tree-Ring Lab, Lamont
983 Doherty Earth Observatory of Columbia University, Palisades, NY.
984 Cook, E.R., R. Seager, J. Kushnir, and Coauthors, 2015: Old world megadroughts and
985 pluvials during the Common Era. *Science Advances*, **1**, e1500561, DOI:
986 10.1126/sciadv.1500561.
987 Durkee, J.D., J.D. Frye, C.M. Fuhrmann, M.C. Lacke, H.G. Jeong, T.L. Mote, 2008: Effects of
988 the North Atlantic Oscillation on precipitation-type frequency and distribution in the
989 eastern United States. Theor Appl Climatology **94**, 51-65.
990 Edwards, D.C., and T.B. McKee, 1997: Characteristics of 20th century drought in the United
991 States at multiple time scales. Climatology Report No. 97-2, Colorado State Univ., Ft. Collins,
992 CO.
993 Elliott, K.J., C.F. Miniat, N. Pederson, and S.H. Laseter, 2015: Forest tree growth response to
994 hydroclimatic variability in the southern Appalachians. *Global Change Biology*, **21**, 4627-
995 4641.

Accepted for publication in *Journal of Climate*. DOI 10.1175/JCLI-D-19-0270.1.

Enfield, D.B., A. M. Mestas-Nunez, and P.J. Trimble, 2001: The Atlantic multidecadal oscillation and it's relation to rainfall and river flows in the continental U.S. *Geophys. Res. Lett.,* **28**, 2077-2080.

Fye F.K., D.W. Stahle, E.R. Cook, 2003: Paleoclimatic analogs to 20th century moisture regimes across the USA. *Bull. Am. Meteoro. Soc*., **84**, 901–909

Fye, F.K., D.W. Stahle, E.R. Cook, and M.K. Cleaveland, 2006: NAO influence on sub-decadal moisture variability over central North America. *Geophys. Res. Lett.,* **33**, L15707, doi:10.1029/2006GL026656.

Fritts, H.C., 1966: Growth-rings of trees: Their correlation with climate. *Science*, **154**, 973–979.

Fritts, H.C., J.E. Mosiman, and C.P. Bottorff. 1969: A revised computer program for standardizing tree-ring series. *Tree Ring Bull.,* **29**, 15–20.

Fritts, H. C., 1971: Dendroclimatoloty and dendroecology. *Quaternary Research*, **1**, 419-449.

Griffin, R.D. C.A. Woodhouse, D.M. Meko, D.W. Stahle, H.L. Faulstich, C. Carrillo, R. Touchan, C.L. Castro, and S.W. Leavitt, 2013: North American monsoon precipitation reconstructed from tree rings. *Geophys. Res. Lett.,* **40**, doi:10.1002/grl.50184.

Grissino-Mayer, H.D., and H.C. Fritts, 1997: The International Tree-Ring Data Bank: An enhanced global database serving the global scientific community. *Holocene,* **7**, 235–238.

Groisman, P.Ya., R.W. Knight, T.R. Karl, D.R. Easterling, B. Sun, and J.H. Lawrimore, 2004: Contemporary changes of the hydrological cycle over the contiguous United States: Trends derived from in situ observations. *J. Hydrometeor*., **5**, 64–85.

Groisman, P.Ya., R.W. Knight, D.R. Easterling, T.R. Karl, G.C. Hegerl, and V.N. Razuvaev, 2005: Trends in intense precipitation in the climate record. *J. Climate*, **18**, 1326-1350.

Accepted for publication in *Journal of Climate*. DOI 10.1175/JCLI-D-19-0270.1.

1019 Guttman, N.B., J.R.M. Hosking, and J.R. Wallis, 1993: Regional precipitation quantile values
1020 for the continental United States computed from L-Moments. *J. Clim*, **6**, 2326-2340.
1021 Guttman, N.B., 1999: Accepting the standardized precipitation index: A calculation
1022 algorithm. *J. Am. Water Resources Assoc*., **35**, 311-322.
1023 Harris, I., P.D. Jones, T.J. Osborn, D.H. Lister, 2014: Updated high resolution grids of
1024 monthly climatic observations - the CRU TS3.10 dataset. *Int. J. Climatology,* **34**, 623-642.
1025 Herweijer, C., R. Seager, and E.R. Cook, 2006: North American droughts of the mid to late
1026 nineteenth century: a history, simulation and implication for Mediaeval drought. *Holocene*,
1027 **16**,159–171
1028 Hinkley, D.A. 1977: On quick choice of power transformation. *Applied Statistics,* **26**, 67-69.
1029 Hoaglin, D.C., F. Mosteller, J.W. Tukey, 2000: *Understanding Robust and Exploratory Data*
1030 *Analysis*. Wiley, 472 pp.
1031 Hoerling, M., J. Eischeid, J. Perlwitz, X-W. Quan, K. Wolter, L. Cheng, 2016: Characterizing
1032 recent trends in U.S. heavy precipitation. J. Climate, 29, 2313-2332.
1033 Hosking, J.R.M., 1990: L-moments: Analysis and estimation of distributions using linear
1034 combinations of order statistics. *Roy. Stat. Soc. London*, **52**, 105-124.
1035 Hu, Q., and S. Feng, 2009: Influence of the Arctic oscillation on central United States
1036 summer rainfall. *J. Geophys. Res*., **115**, D01102, doi:10.1029/2009JD011805.
1037 Hurrell, J. W., Y. Kushnir, and G. Ottersen, 2003: An overview of the North Atlantic
1038 oscillation. *The North Atlantic Oscillation: Climatic Significance and Environmental Impact*,
1039 J.W. Hurrell, Y. Kushnir, G. Ottersen, M. Visbeck, and M.H. Visbeck, Eds., *Geophysical*
1040 *Monograph Series*, American Geophysical Union, Washington, 1-35 doi:10.1029/134GM01.

Accepted for publication in *Journal of Climate*. DOI 10.1175/JCLI-D-19-0270.1.

Hurvich, C.M., and C.L. Tsai. 1989. Regression and time series model selection in small samples. *Biometrika*, **76**, 297-307.

LeBlanc, D.C., and D.W. Stahle, 2015: Radial growth response of four oak species to climate in eastern and central North America. *Canadian J. Forest Res.,* **45**, 1-12.

Marlon, J.R., N. Pederson, and Coauthors, 2017: Climatic history of the northeastern United States during the past 3000 years. *Climate of the Past*, **13**, 1355-1379.

McCabe, G.J., M.A. Palecki, and J.L. Betancourt, 2004: Pacific and Atlantic influences on drought frequency in the United States. *Proc. Nat. Acad. Sci*., **101**, 4136-4141.

Meko, D.M, 1981: Applications of Box-Jenkins Methods of time-series analysis to reconstruction of drought from tree rings. Ph.D. Dissertation, University of Arizona, Tucson.

Meko, D.M., E.R. Cook, D.W. Stahle, C.W. Stockton, and M.K. Hughes, 1993: Spatial patterns of tree growth anomalies in the United States and southeastern Canada. *J. Climate*, **6**, 1773-1786.

Meko, D.M., C.W. Stockton, W.R. Boggess, 1995: The tree-ring record of severe sustained drought. *Water Resources Bull.*, **31**, 789–801

Meko, D.M., and C.H. Baisan, 2001: Pilot study of latewoodwidth of conifers as an indicator of variability of summer rainfall in the North American monsoon region. *Int. J. Climatology*, **21**, 697–708.

Meko, D.M., D.W. Stahle, D. Griffin, T.A. Knight, 2011: Inferring precipitation-anomaly gradients from tree rings. *Quaternary International* **235**, 89-100.

Melvin, T.M., K.R. Briffa, K. Nicolussi, and M. Grabner, 2007: Time-varying-response smoothing. *Dendrochronologia*, 25, 65–69.

Accepted for publication in *Journal of Climate*. DOI 10.1175/JCLI-D-19-0270.1.

Melvin, T.M., and K.R. Briffa, 2008. A "signal-free" approach to dendroclimatic standardization. *Dendrochronologia,* **26**, 71-86.

Mitchell, T.D., and P. D. Jones, 2005: An improved method of constructing a database of monthly climate observations and associated high-resolution grids. *International Journal of Climatology*, **25**, 693–712.

Mo, K.C., and D.P. Lettenmaier, 2015: Heat wave flash droughts in decline. *Geophys. Res. Lett*., **42**, 2823–2829, doi:10.1002/2015GL064018.

Namias, J., 1982; Anatomy of Great Plains protracted heat waves (especially the 1980 U.S. summer drought). *Monthly Weather Review*, **110**, 824-838.

New, M., M. Hulme, and P. Jones, 2000: Representing twentieth-century space–time climate variability. Part II: Development of 1901–96 monthly grids of terrestrial surface climate. *J. Climate*, **13**, 2217–2238.

Newby, P.E., B.N. Shuman, J.P. Donnelly, K.B. Karnauskas, and J. Marsicek, 2014: Centennial-to-millennial hydrologic trends and variability along the North Atlantic Coast, USA, during the Holocene. *Geophys Res. Lett*., **41**, 4300–4307, doi:10.1002/ 2014GL060183.

Ning, L., and R.S. Bradley, 2016: NAO and PNA influences on winter temperature and precipitation over the eastern United States in CMIP5 GCMs. *Climate Dynamics*, **46**, 1257-1276.

Palmer, W.C., 1965: *Meteorological Drought*. Research Paper No. 45, US Dept Commerce, Weather Bureau.

Palmer, J.G., Cook, E., Turney, C., Allen, K., Fenwick, P., Cook, B., O'Donnell, A., Lough, J., Grierson, P., and Baker, P, 2015: Drought variability in the eastern Australia and New Zealand summer drought atlas (ANZDA, CE 1500-2012) modulated by the Interdecadal

Accepted for publication in *Journal of Climate*. DOI 10.1175/JCLI-D-19-0270.1.

Pacific Oscillation. *Environmental Research Letters*, **10**, https://doi:10.1088/1748-9326/10/12/124002.

Pederson, G.T., S.T. Gray, C.A. Woodhouse, J.L. Betancourt, D.B. Fagre, J.S. Littell, E. Watson, B.H. Luckman, L.J. Graumlich, 2011: The unusual nature of recent snowpack declines in the North American cordillera. *Science*, **333**, 332-335.

Pederson, N., A. Bell, E. Cook, U. Lall, N. Devenini, R. Seager, K. Eggelston and K. Vranes, 2013: Is an epic pluvial masking the water insecurity of the greater New York City region? *J. Climate*, **26**, 1339-1354.

Quan, N.T. 1988. The prediction sum of squares as a general measure for regression diagnostics. *J. Business & Economic Statistics*, **6**, 501-504.

Salzer, M.W., A.G. Bunn, N.E. Graham, and M.K. Hughes, 2014: Five millennia of paleotemperature from tree-rings in the Great Basin, USA. *Climate Dynamics*, **42**, 1517–1526.

Schneider, U., A. Becker, P. Finger, A. Meyer-Christoffer, M. Ziese, Markus, 2018: GPCC Full Data Monthly Product Version 2018 at 0.5°: Monthly Land-Surface Precipitation from Rain-Gauges built on GTS-based and Historical Data.
DOI: 10.5676/DWD_GPCC/FD_M_V2018_050

Schulman, E., 1942: Dendrochronology in pines of Arkansas. *Ecology*, **23**, 309–318.

Seager, R., 2007: The turn of the century North American drought: Global context, dynamics and past analogues. *J. Climate*, **20**, 5527-5552.

Seager, R., N. E. Graham, C. Herweijer, A. Gordon, Y. Kushnir and E. Cook, 2007: Blueprints for Medieval hydroclimate. *Quaternary Sci. Rev*., **26**, 2322-2336.

Accepted for publication in *Journal of Climate*. DOI 10.1175/JCLI-D-19-0270.1.

1109 Seager, R., N. Pederson, Y. Kushnir, J. Nakamura and S. Jurburg, 2012: The 1960s drought
1110 and subsequent shift to a wetter climate in the Catskill Mountains region of the New York
1111 City watershed. *J. Climate*, **25**, 6721-6742.
1112 Seager, R. and M. P. Hoerling, 2014: Atmosphere and ocean origins of North American
1113 droughts. *J. Climate*, **27**, 4581-4606.
1114 Shoemaker, L.H., 2003: Fixing the *F* test for equal variances. *Am. Statistician*, **57**, 105-114.
1115 Shuman, B.N., and J. Marsicek, 2016: The structure of Holocene climate change in mid-
1116 latitude North America. *Quaternary Sci. Rev*., **141**, 38-51.
1117 Smerdon, J.E., Cook, B.I., Cook, E.R., and Seager, R., 2015: Bridging past and future climate
1118 across paleoclimatic reconstructions, observations, and models: A hydroclimate case study.
1119 *Journal of Climate*, **28**, 3212-3231.
1120 Smerdon, J. E. and others, 2017: Comparing proxy and model estimates of hydroclimate
1121 variability and change over the Common Era. *Climate of the Past*, **13**, 1851-1900.
1122 St. George, S., 2014. An overview of tree-ring width records across the Northern
1123 Hemisphere. *Quaternary Sci. Rev*., **95**, 132–150.
1124 Stahle, D.W., and J.S. Dean, 2011: North American tree rings, climatic extremes, and social
1125 disasters. *Dendroclimatology: Progress and Prospects*, M.K. Hughes, T.W. Swetnam, H.F. Diaz,
1126 editors. Developments in Paleoenvironmental Research, Vol. 11, Springer, pp. 297-327.
1127 Stahle, D.W., E.R. Cook, M.K. Cleaveland, M.D. Therrell, D.M. Meko, H.D. Grissino-Mayer, E.
1128 Watson, and B.H., Luckman, 2000: Tree-ring data document 16th century megadrought
1129 over North America. *Eos, Transactions Am. Geophys. Union* **81**(12), 212, 125.
1130 Stahle, D.W., F.K. Fye, and E.R. Cook, 2007: Tree-ring reconstructed megadroughts over
1131 North America since AD 1300. *Climatic Change,* **83**, 133-149.

Accepted for publication in *Journal of Climate*. DOI 10.1175/JCLI-D-19-0270.1.

1132 Stahle, D.W., M.K. Cleaveland, H. Grissino-Mayer, R.D. Griffin, F.K. Fye, M.D. Therrell, D.J.
1133 Burnette, D.M. Meko, and J. Villanueva Diaz, 2009: Cool and warm season precipitation
1134 reconstructions over western New Mexico. *J. Climate,* **22**, 3729-3750.
1135 Stahle, D.W., R. D. Griffin, D. M. Meko, M. D. Therrell, J. R. Edmondson, M. K. Cleaveland, L. N.
1136 Stahle, D. J. Burnette, J. T. Abatzoglou, K. T. Redmond, M. D. Dettinger, and D. R. Cayan, 2013.
1137 The blue oak woodlands of California: longevity and hydroclimatic history. *Earth*
1138 *Interactions,* **17**(12), 1-23, DOI: 10.1175/2013EI000518.1.
1139 Stahle, D.W., E.R. Cook, D.J. Burnette, J. Villanueva, J. Cerano, J.N. Burns, R.D. Griffin, B.I.
1140 Cook, R. Acuna, MCA Torbenson, and P. Sjezner, 2016: The Mexican Drought Atlas: Tree-
1141 ring reconstructions of the soil moisture balance during the late Pre-Hispanic, Colonial, and
1142 Modern Eras. *Quaternary Sci. Rev.,* **149**, 34-60.
1143 Swetnam, T.W., C.H. Baisan, A.C. Caprio, P.M. Brown, R. Touchan, R.S. Anderson, and D.J.
1144 Hallett, 2009: Multi-millennial fire history of the Giant Forest, Sequoia National Park,
1145 California, USA. Fire Ecology, 5, 120-150.
1146 Therrell, M.D., D.W. Stahle, M.K. Cleaveland, and J. Villanueva-Diaz, 2002. Warm season tree
1147 growth and precipitation over Mexico. *J. Geophys. Res.,* **107**(D14), ACL 6-1 to 6-8.
1148 Thom, H.C.S., 1966: Some methods of climatological analysis. *WMO Tech Note No. 81*, 53 pp.
1149 Thompson, D.W.J., and J.M. Wallace, 2000: Regional climate impacts of the Northern
1150 Hemisphere annular mode. *Science*, **293**, 85-89.
1151 Tierney, J.E., Abram, N.J., Anchukaitis, K.J., Evans, M.N., Giry, C., Kilbourne, K.H., Saenger,
1152 C.P., Wu, H.C., and Zinke, J., 2015: Tropical sea surface temperatures for the past four
1153 centuries reconstructed from coral archives. *Paleoceanography*, **30**, 226–252.
1154 https://doi: 10.1002/2014PA002717.

Accepted for publication in *Journal of Climate*. DOI 10.1175/JCLI-D-19-0270.1.

Torbenson, M.C.A., D.W. Stahle, J. Villanueva, E.R. Cook, and D.R. Griffin, 2016. The relationship between earlywood and latewood tree-growth across North America. *Tree-Ring Research,* **72**, 53-66.

Torbenson, MCA, and D.W. Stahle, 2018. The relationship between cool and warm season moisture over the central United States, 1685-2015. *J. Climate,* **31**, 7909-7924.

Torbenson, M.C.A., D.W. Stahle, I.M. Howard, D.J. Burnette, J. Villanueva-Díaz, E.R. Cook, D. Griffin, 2019: Multidecadal modulation of the ENSO teleconnection to precipitation and tree growth over subtropical North America. *Paleooceanography and Paleoclimatology*, (in press).

USGCRP, 2018: Impacts, Risks, and Adaptation in the United States: *Fourth National Climate Assessment*, Volume II [Reidmiller, D.R., C.W. Avery, D.R. Easterling, K.E. Kunkel, K.L.M. Lewis, T.K. Maycock, and B.C. Stewart (eds.)]. U.S. Global Change Research Program, Washington, DC, USA, 1515 pp. doi: 10.7930/NCA4.2018

Villanueva-Diaz, J., D. Stahle, B. Luckman, J. Cerano-Paredes, M. Therrell, M.K. Cleaveland, and E. Cornejo-Oviedo, 2007: Winter-spring precipitation reconstruction from tree rings for northeast Mexico. *Climatic Change,* **83**, 117-131.

Watson, E., and B.H. Luckman, 2002: The dendroclimatic signal in Douglas-fir and ponderosa pine tree-ring chronologies from the southern Canadian Cordillera. *Can. J. Forest Res.*, **32**, 1858-1874.

Welsh, C., Smith, D.J., and Coulthard, B. L. (2019). Tree ring records unveil long term influence of the Pacific Decadal Oscillation on snowpack dynamics in the Stikine River basin, northern British Columbia. *Hydro. Processes*, **33**, 720-736.

Accepted for publication in *Journal of Climate*. DOI 10.1175/JCLI-D-19-0270.1.

Whan, K., and F. Zwiers, 2017: The impact of ENSO and the NAO on extreme winter precipitation in North America in observations and regional climate models. *Climate Dynamics*, **48**, 1401-1411.

Williams, A.P., B. I. Cook, J. E. Smerdon, D. A. Bishop and R. Seager, 2017: The 2016 southeastern US drought: an extreme departure from centennial wetting and cooling. *J. Geophys. Res.-Atmos.*, doi:10.1002/2017JD027523.

Wolter, K., and M.S. Timlin, 2011: El Nino/southern Oscillation behaviour since 1871 as diagnosed in an extended multivariate ENSO index (MEI.ext). *Int. J. Climatology,* **31**, 1074-1087.

Woodhouse, C.A., K.E. Kunkel, D.R. Easterling, and E.R. Cook, 2005: The twentieth-century pluvial in the western United States. *Geophys. Res. Lett.*, **32**, L07701, doi:10.1029/2005GL022413.

Accepted for publication in *Journal of Climate*. DOI 10.1175/JCLI-D-19-0270.1.

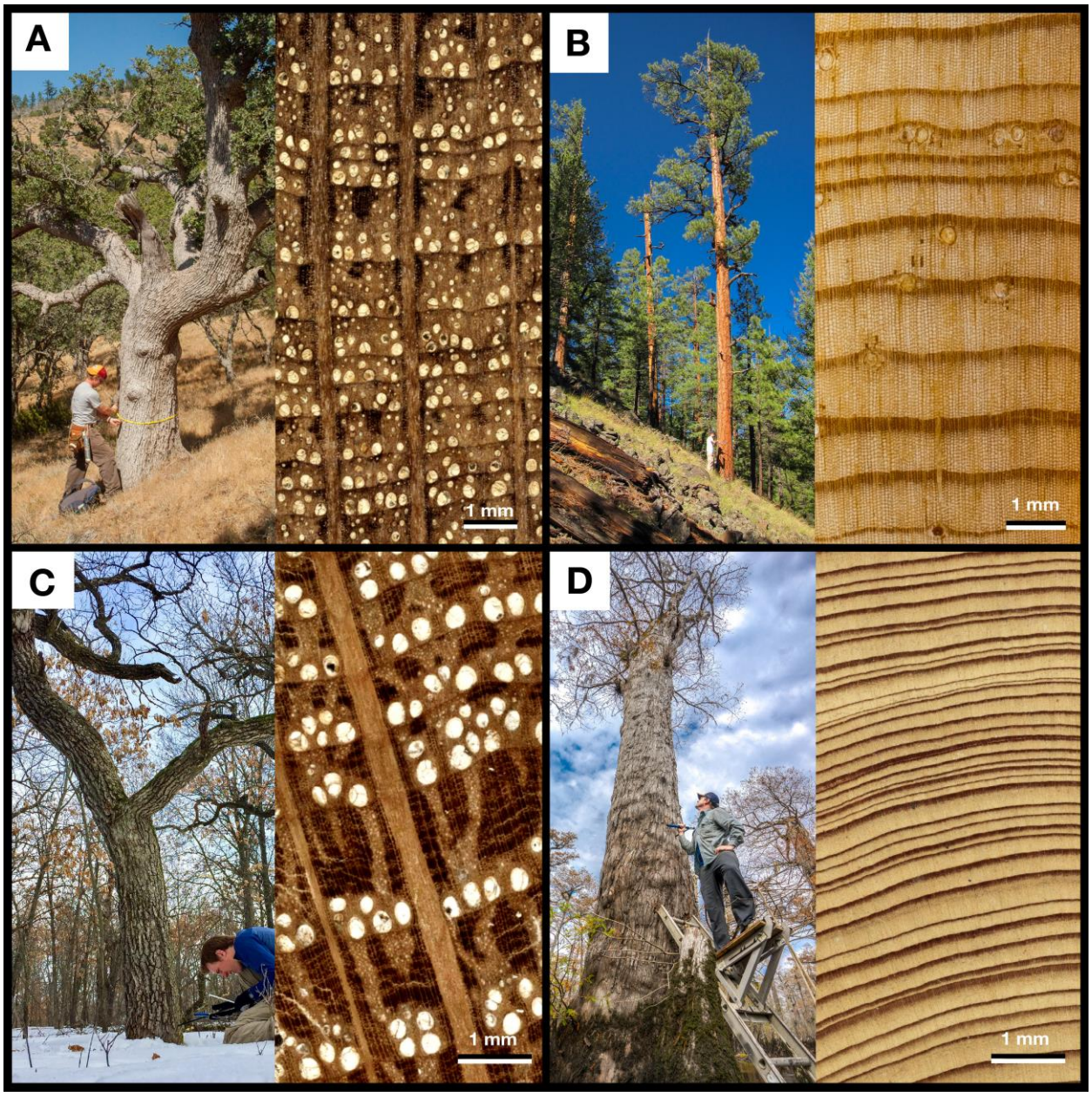

Figure 1. Four important tree species for seasonal precipitation reconstruction are illustrated, along with photomicrographs of their annual rings that display prominent variability in earlywood and latewood width [a: blue oak (*Quercus douglasii*); b: ponderosa pine (*Pinus ponderosa*); c: bur oak (*Q. macrocarpa*); d: bald cypress (*Taxodium distichum*)].

Accepted for publication in *Journal of Climate*. DOI 10.1175/JCLI-D-19-0270.1.

1197

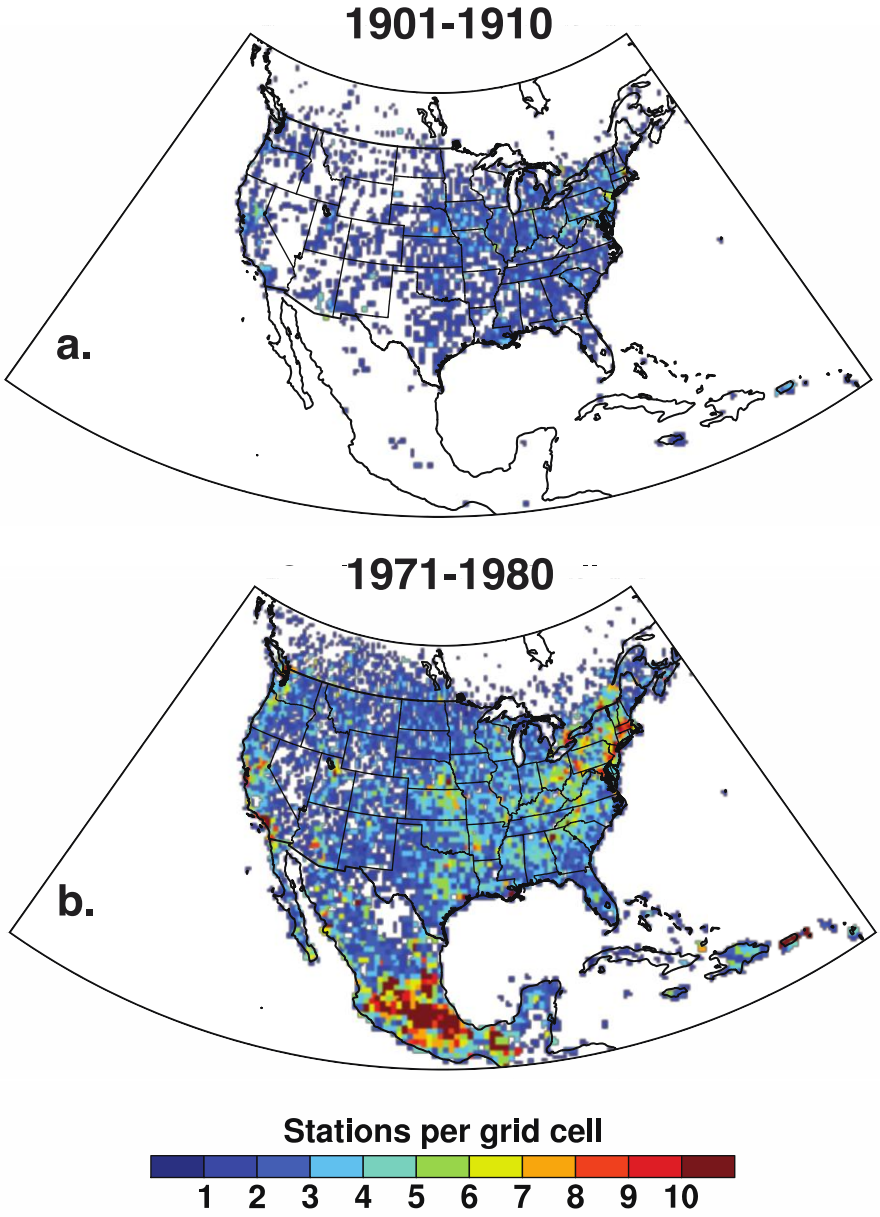

1198

1199 **Figure 2.** The availability of instrumental precipitation measurements in the GPCC-Full

1200 Data set is illustrated for two decades in the early and late 20th century by the median

1201 number of stations per 0.25° grid cell.

1202

Accepted for publication in *Journal of Climate*. DOI 10.1175/JCLI-D-19-0270.1.

1203

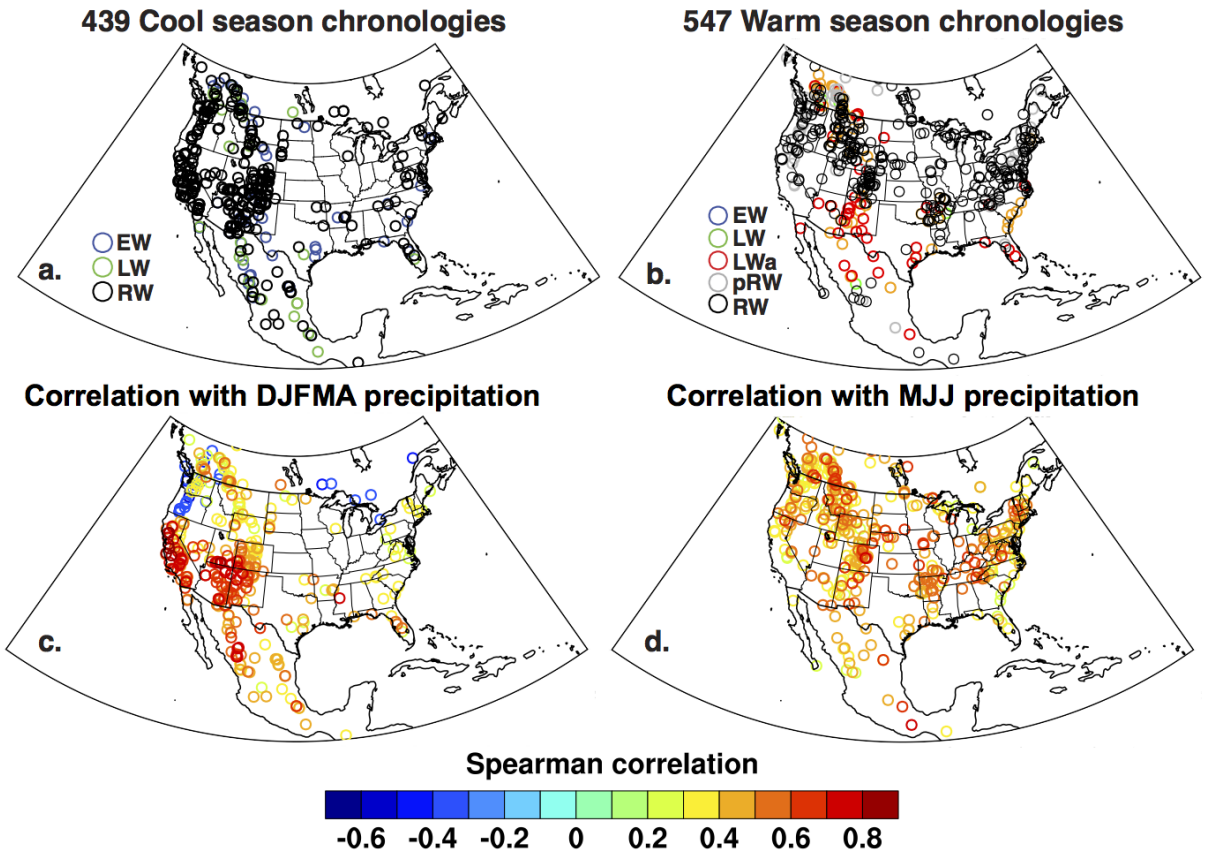

1204

1205 **Figure 3.** (a) Site locations for the 439 tree-ring chronologies that are discretely correlated
1206 with cool season precipitation (DJFMA), and (b) the 547 chronologies discretely correlate
1207 with warm season totals (MJJ). The type of chronology used is also indicated (EW,
1208 earlywood; LW, latewood; LWa, adjusted latewood; RW, total ring width; pRW, ring width
1209 with a prior year warm season signal). The Spearman rank order correlation computed
1210 between each chronology and the nearest GPCC precipitation grid point is mapped for
1211 DJFMA (c) and MJJ totals (d).

1212

Accepted for publication in *Journal of Climate*. DOI 10.1175/JCLI-D-19-0270.1.

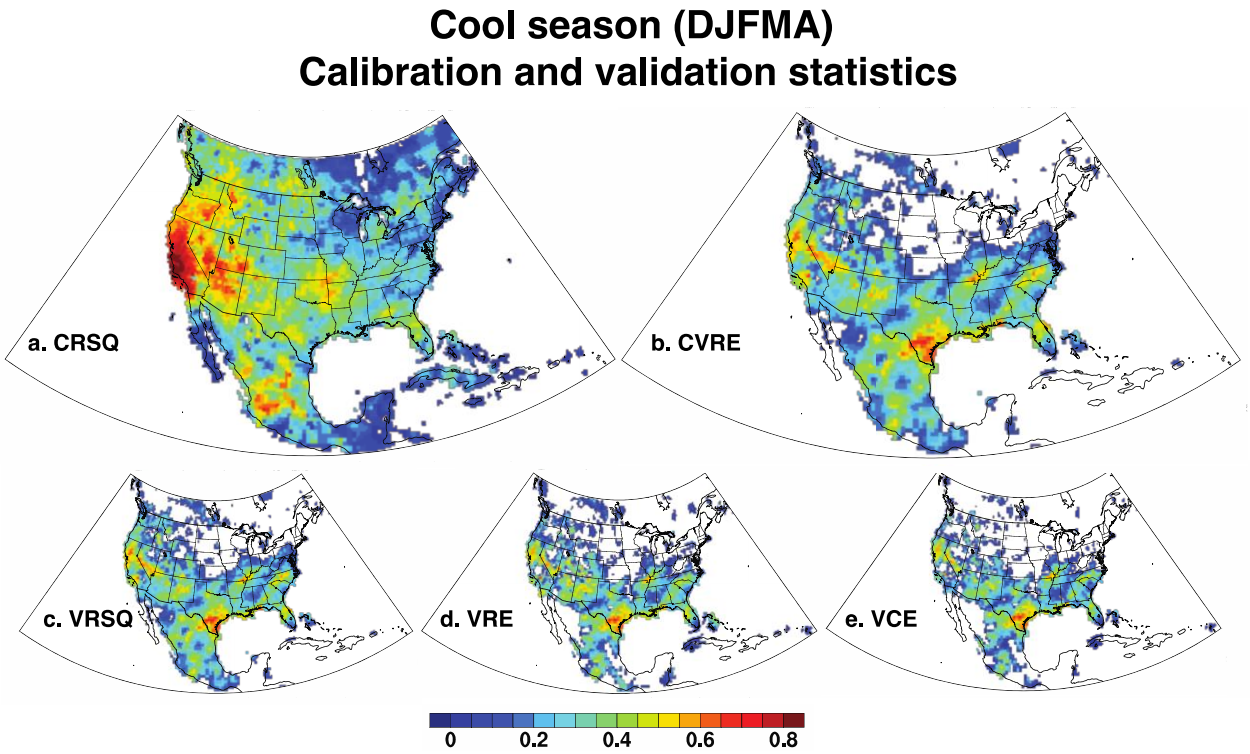

Figure 4. The calibration and validation statistics computed for the tree-ring estimates of cool season (DJFMA) precipitation totals are mapped for the 6,812 grid points over North America. The calibration interval was 1928-1978 and the validation interval was 1901-1927 (calibration statistics: CRSQ = coefficient of multiple determination, CVRE = cross validation reduction of error; validation statistics: VRSQ = Pearson correlation coefficient squared, VRE = reduction of error, VCE = coefficient of efficiency).

Accepted for publication in *Journal of Climate*. DOI 10.1175/JCLI-D-19-0270.1.

1222

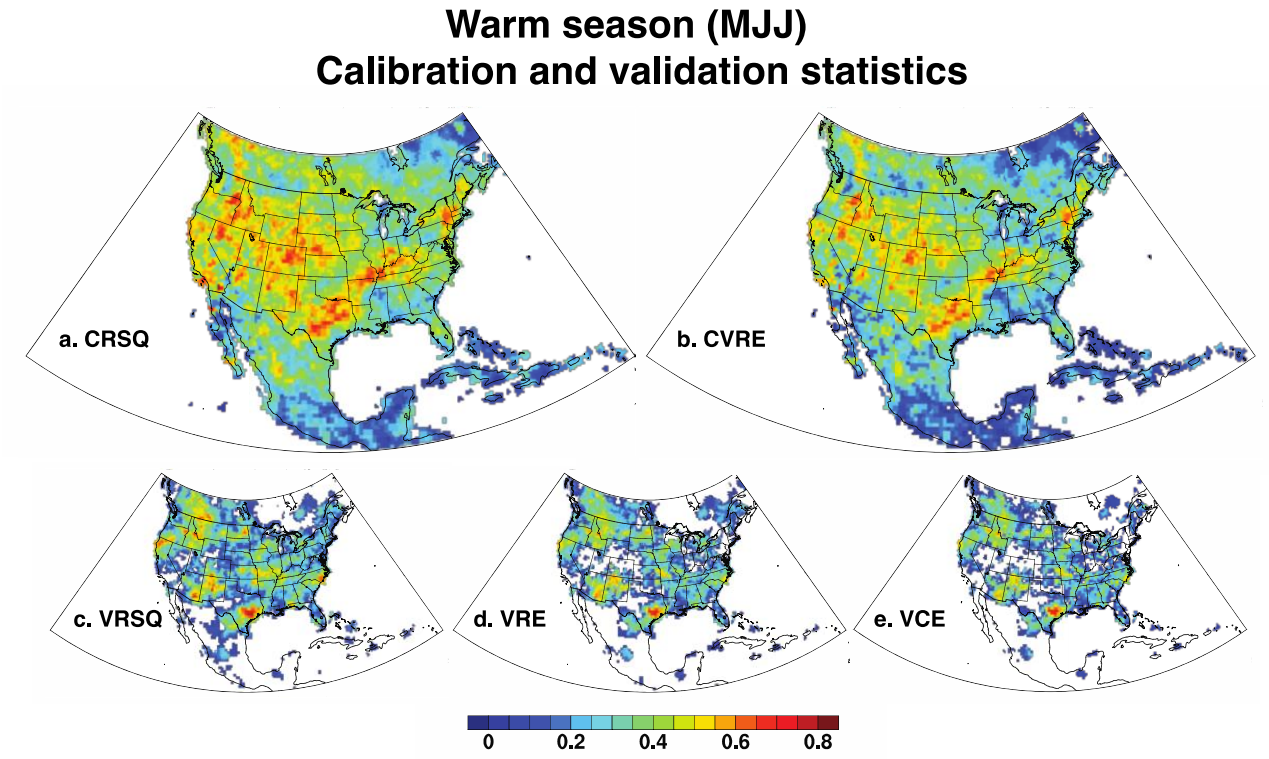

1223

1224 **Figure 5.** Same as Figure 4 for the tree-ring reconstructions of warm season (MJJ)

1225 precipitation totals.

1226

Accepted for publication in *Journal of Climate*. DOI 10.1175/JCLI-D-19-0270.1.

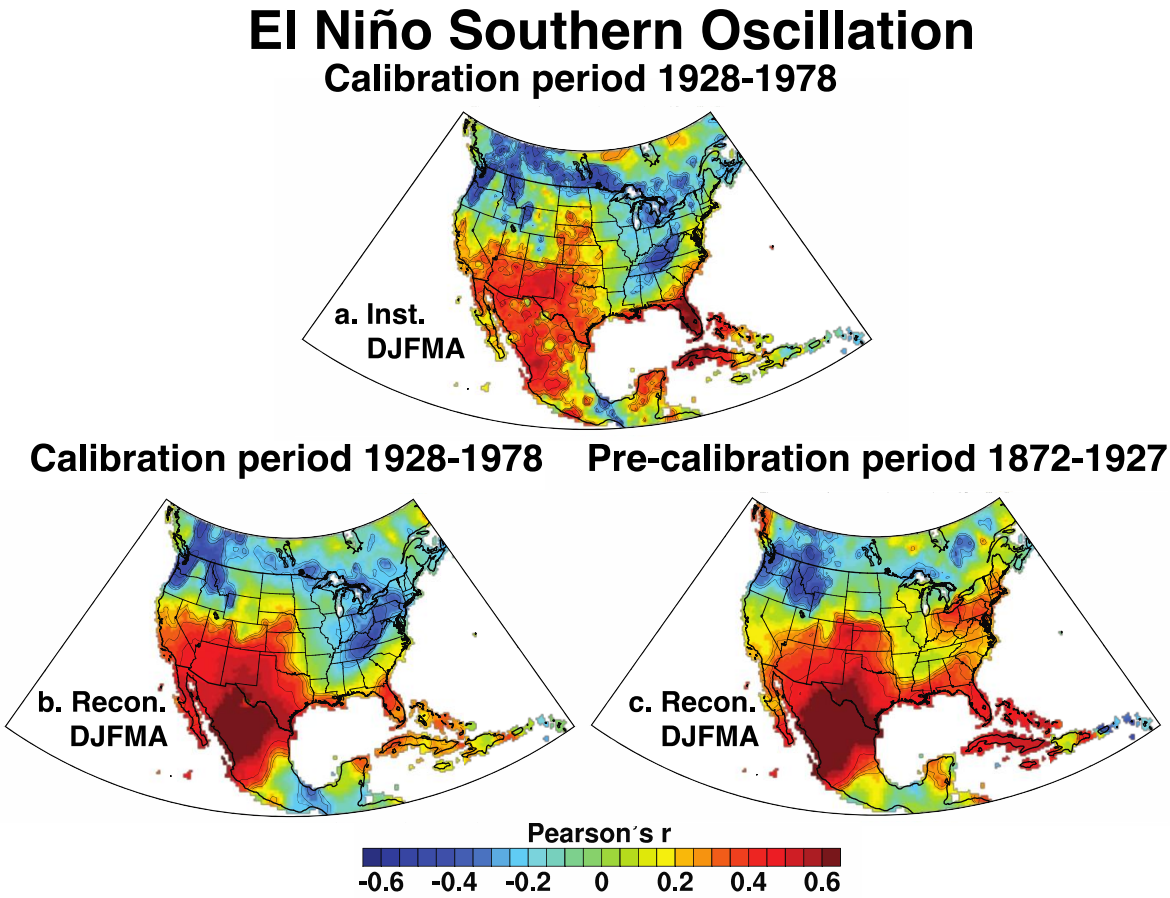

Figure 6. The correlation between the November-February extended Multivariate ENSO Index (Wolter and Timlin 2009) and gridded instrumental (a) and reconstructed cool season precipitation totals (b) for the period 1928-1978 are mapped. (c) Same as (b) for the pre-calibration period from 1872-1927 using tree-ring reconstructed cool season totals and the instrumental eMEI. Four levels of significance are indicated by the contours (p = 0.10, 0.05, 0.01, 0.001). Regions without reconstructed validation skill in the early 20th century are mapped in Figure 4, but the similarity between instrumental and reconstructed patterns of ENSO correlation (a-c) lend credibility to the reconstructions even in some areas without statistical validation from 1901-1927.

Accepted for publication in *Journal of Climate*. DOI 10.1175/JCLI-D-19-0270.1.

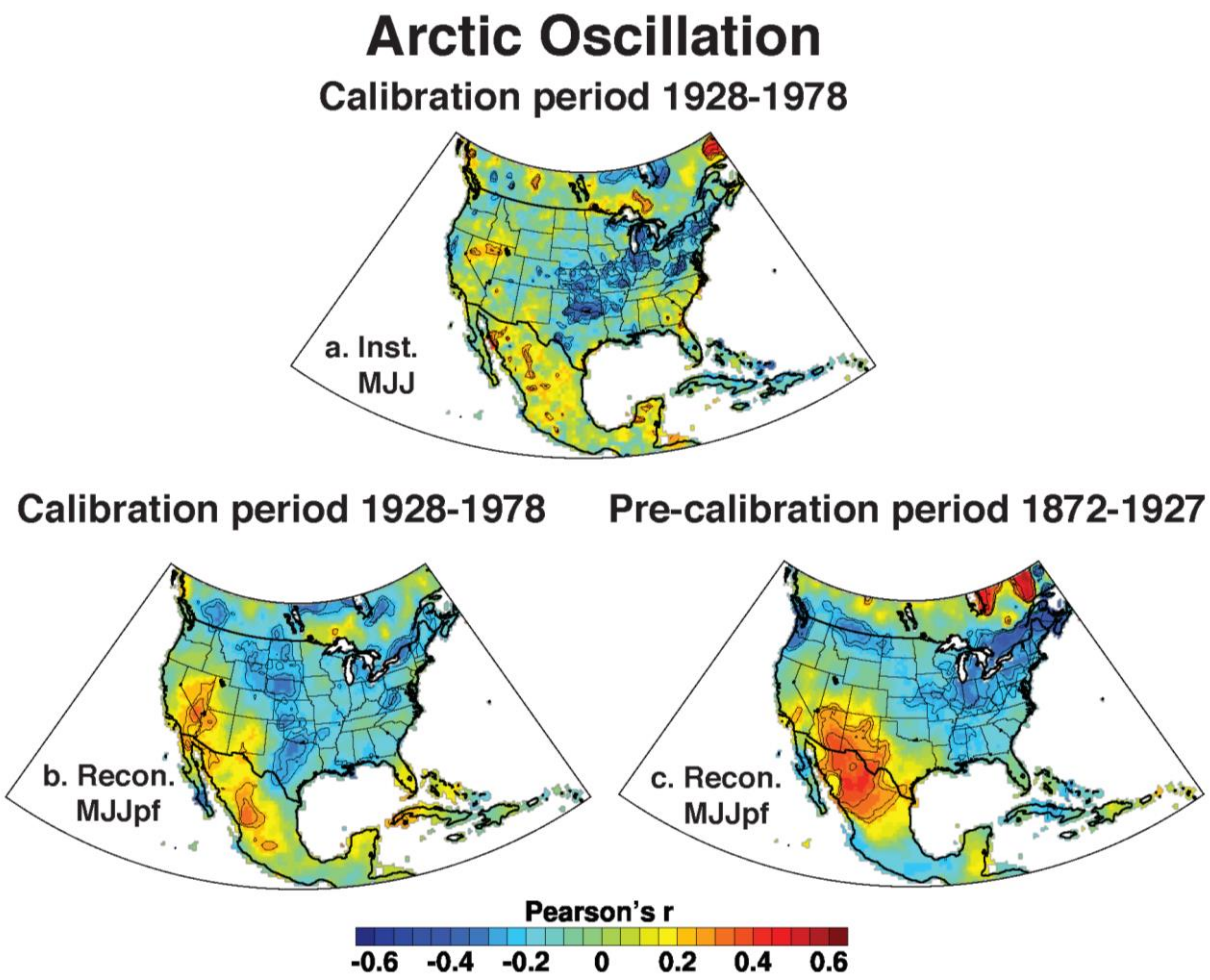

Figure 7. Same as Figure 6 for the Arctic Oscillation Index averaged for May and June, correlated with instrumental MJJ (a) and reconstructed MJJpf precipitation totals (b,c).

Accepted for publication in *Journal of Climate*. DOI 10.1175/JCLI-D-19-0270.1.

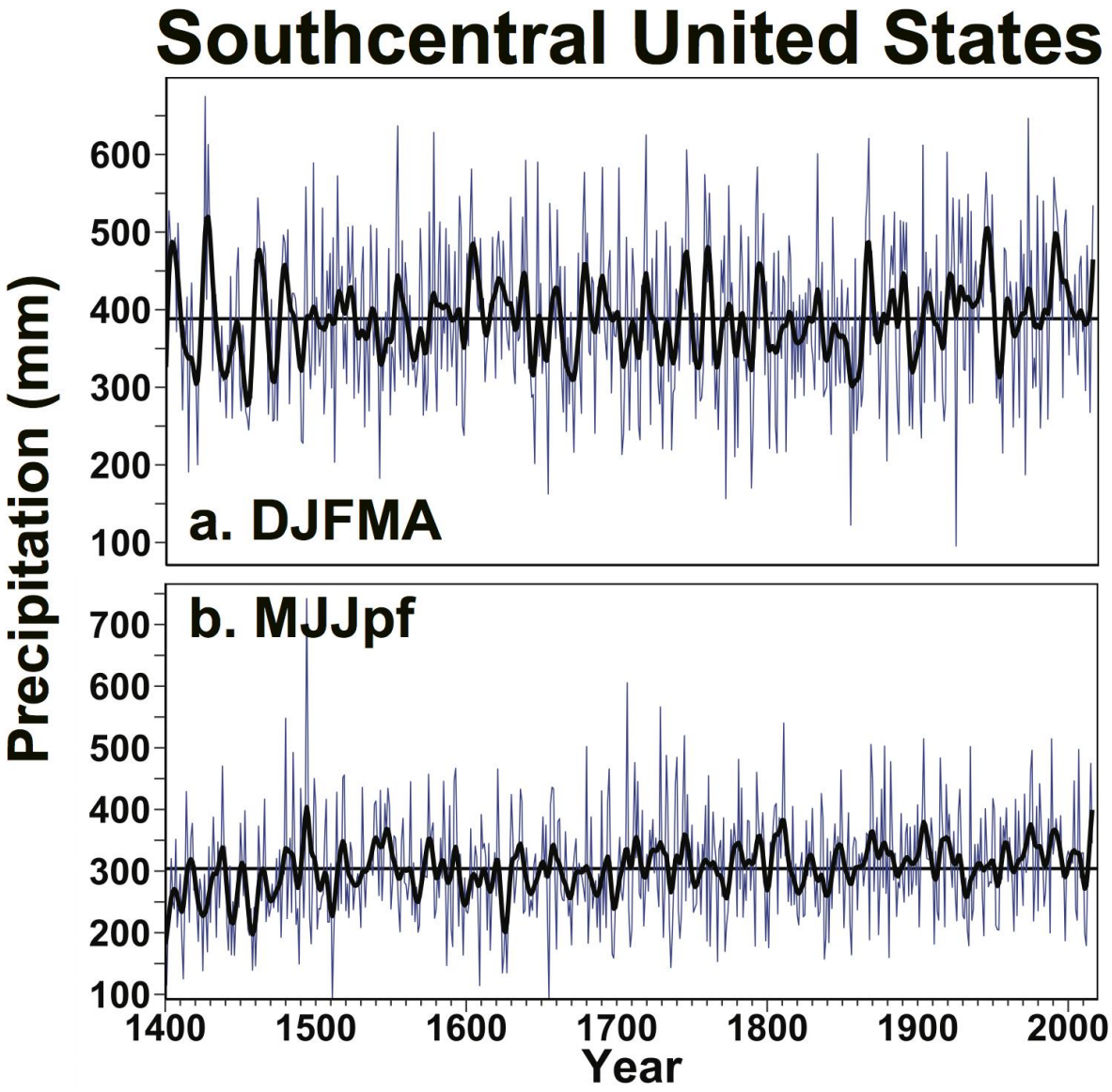

Figure 8. Tree-ring reconstructed cool (a, DJFMA) and warm season precipitation totals (b, MJJpf) are plotted from 1400-2016 for the southcentral United States (29-39°N, 90-100°W). Annual values are illustrated in blue. The black curve is a fitted spline emphasizing decadal variability. Regional average reconstructions are plotted for eight other subregions of North America in Figure SM-12.

Accepted for publication in *Journal of Climate*. DOI 10.1175/JCLI-D-19-0270.1.

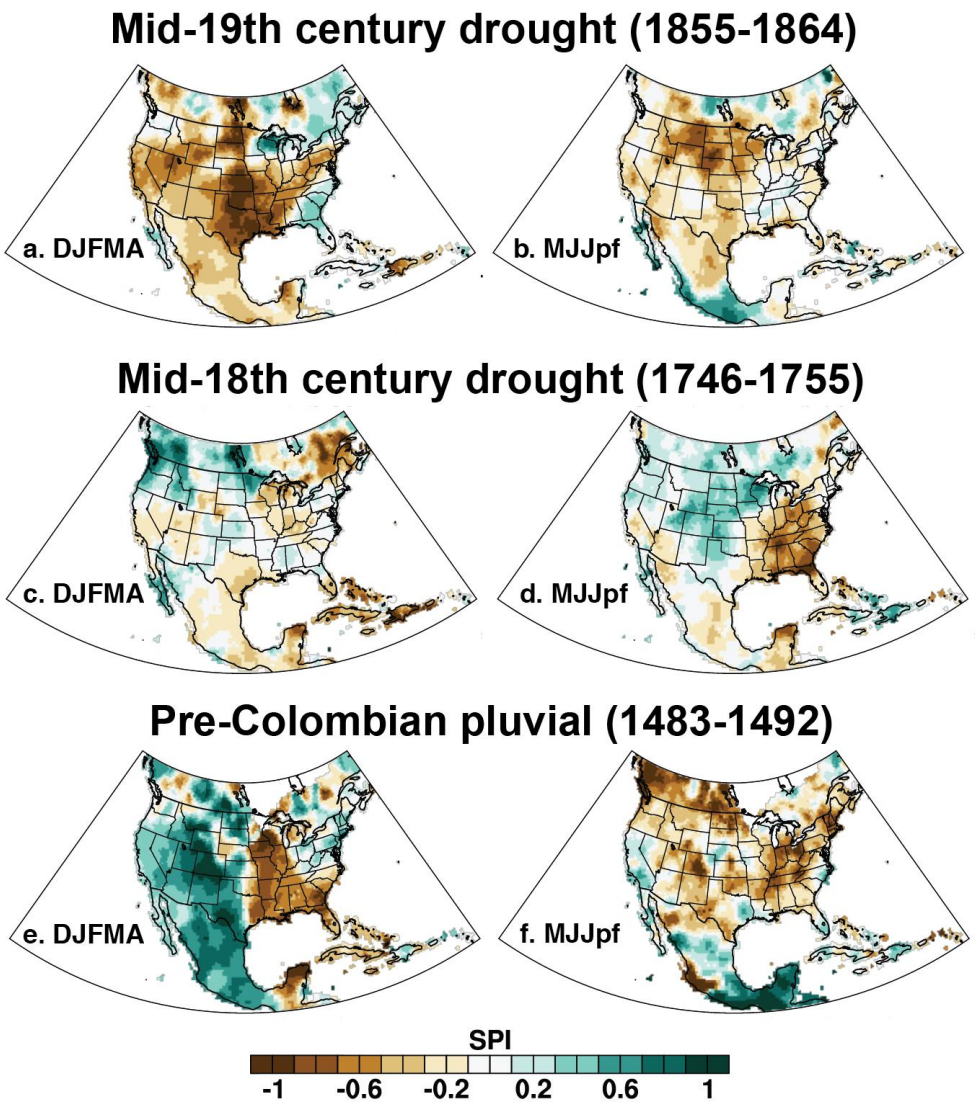

Figure 9. Tree-ring reconstructed cool (a) and persistence-free warm season standardized precipitation indices (SPI; b) during the mid-19th Century Drought are averaged and mapped for the decade from 1855 to 1864. The most intense 10-years of the mid-18th Century Drought (1746-1755; c,d) and the Pre-Columbian Pluvial (1483-1492, e,f) are also mapped using SPI for the seasonal precipitation reconstructions.

Accepted for publication in *Journal of Climate*. DOI 10.1175/JCLI-D-19-0270.1.

1259

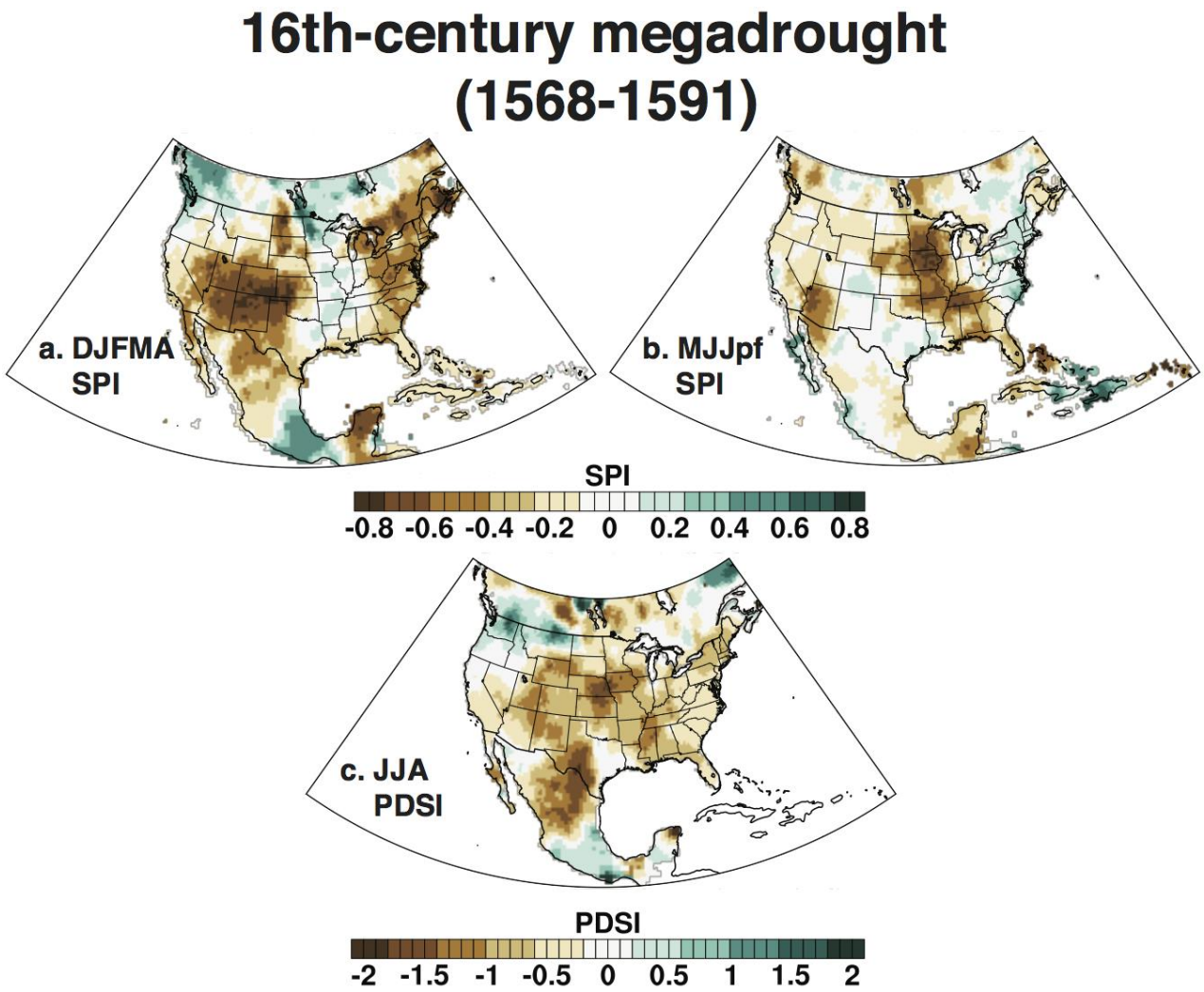

1260

1261 **Figure 10.** (a-b) Same as Figure 9, tree-ring reconstructed SPI for the 24-year interval

1262 from 1568 to 1591 during the 16th Century Megadrought. (c) The tree-ring reconstructions

1263 of summer PDSI for 1568-1591 are also mapped from the North American Drought Atlas

1264 (Cook et al 2010).

1265

Accepted for publication in *Journal of Climate*. DOI 10.1175/JCLI-D-19-0270.1.

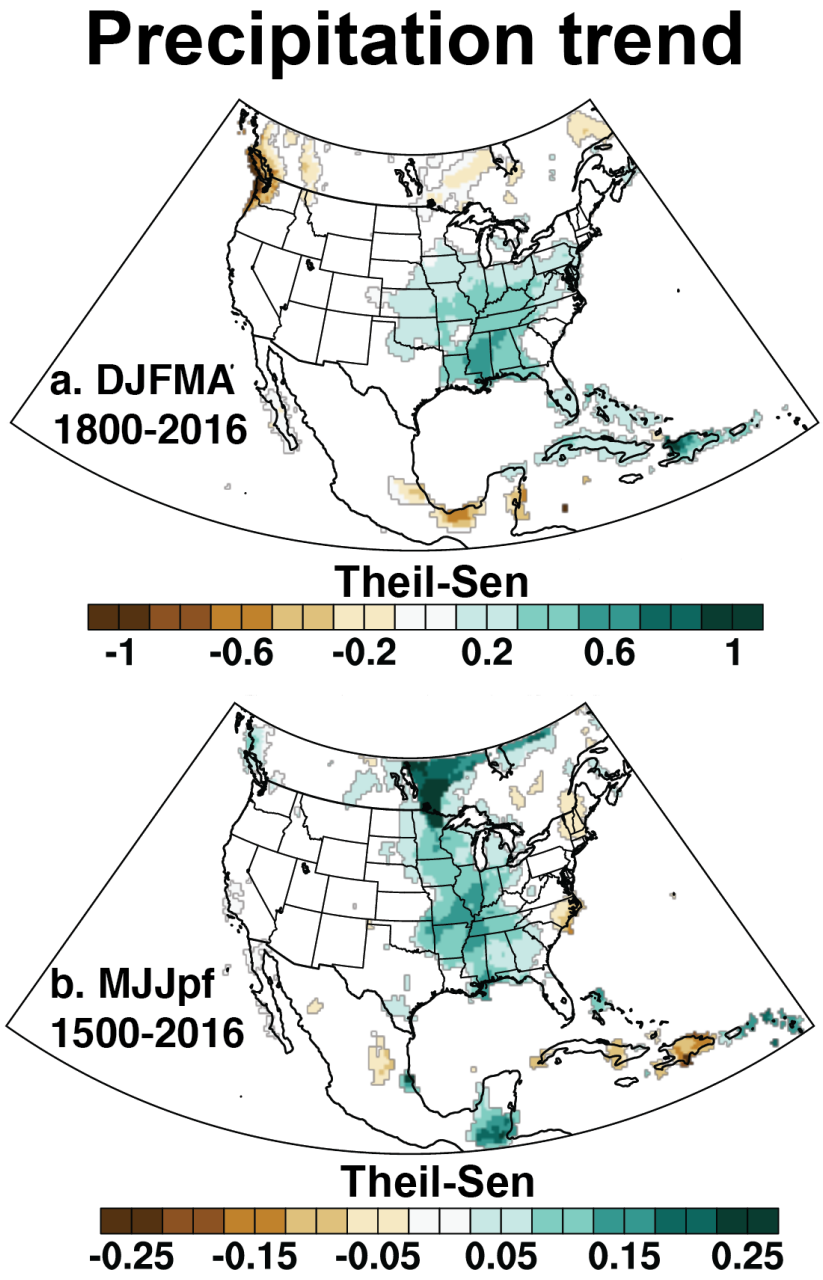

Figure 11. Significant positive trend in reconstructed cool season precipitation has been detected over the eastern United States since 1800 (a), and since 1500 for reconstructed warm season precipitation (b), based on the Theil-Sen slope estimate.

Accepted for publication in *Journal of Climate*. DOI 10.1175/JCLI-D-19-0270.1.